Robotics and Autonomous Systems 60 (2012) 769–788

Contents lists available at SciVerse ScienceDirect

Robotics and Autonomous Systems

journal homepage: www.elsevier.com/locate/robot

# Real-time navigation of mobile robots in problems of border patrolling and avoiding collisions with moving and deforming obstacles

Alexey S. Matveev [a], Chao Wang [b,*], Andrey V. Savkin [b]

[a] Department of Mathematics and Mechanics, Saint Petersburg University, Universitetskii 28, Petrodvoretz, St. Petersburg, 198504, Russia

[b] School of Electrical Engineering and Telecommunications, The University of New South Wales, Sydney 2052, Australia

ARTICLE INFO

*Article history:*
Received 17 November 2011
Received in revised form
13 February 2012
Accepted 17 February 2012
Available online 5 March 2012

*Keywords:*
Real-time navigation
Border patrolling
Guidance
Moving obstacles
Unknown dynamic environment
Nonholonomic under-actuated robots

ABSTRACT

We present a sliding mode based strategy for a unicycle-like robot navigation and guidance. The proposed navigation law is applied to the problems of patrolling the border of a moving and deforming domain and reaching a target through a dynamic environment cluttered with moving obstacles. Mathematically rigorous analysis of the proposed approach is provided. The convergence and performance of the algorithm is demonstrated via experiments with real robots and extensive computer simulation.



## 1. Introduction

For most real life applications of mobile robotics, a basic requirement is the capability to safely operate in dynamic and a priori unknown environments. Despite extensive research, this problem still represents a real challenge, mostly because of numerous uncertainties inherent in this scenario. This trouble can be much enhanced by deficiency in perception abilities and computational power of the robot, as well as by restrictions on its mobility due to nonholonomic kinematic constraints, limited control range, and under-actuation.

Avoidance of collisions with obstacles is a key component of safe navigation. A typical objective is to reach a target through the obstacle-free part of the environment [1]. This may involve bypassing an obstacle, especially a long one, in a close range with a safety margin [2]. This maneuver is similar to border patrolling, which mission is of independent interest for many applications. Many efforts have been undertaken in robotics research for solution of these problems. The obtained rich variety of algorithms can be generally classified into global and local path planners [3].

Global planners (GP) use a priori and sensory information to build a comprehensive model of the environment and to find the best complete trajectory [1]. Within this framework, several techniques (surveyed in e.g., [4,5]) have been developed for dynamic scenes, including nonholonomic planners [6], velocity obstacles [7,4] and state-time space [8,9] approaches. By and large, GP are computationally expensive and hardly suit real-time implementation; NP-hardness, the mathematical seal for intractability, was established for even the simplest problems of dynamic motion planning [10]. GP are also plagued by data incompleteness and erroneousness typical for onboard perception.

Conversely, local planners use onboard sensory data about a nearest fraction of an unknown environment for iterative re-computation of a short-horizon path. This reduces the calculation time and creates a potential for employment in real-time guidance systems. Many of the related techniques, such as the dynamic window [11,12], the curvature velocity [13], and the lane curvature [14] approaches in fact treat the obstacles as static. On the other hand, approaches like velocity obstacles [7,4], collision cones [15], or inevitable collision states [16,17], assume a deterministic knowledge about the obstacle velocity and a moderate rate of its change.

When the planning horizon collapses into a point, local planner acts as a reactive controller: it converts the current observation into the current control. Examples concerning nonholonomic robots include artificial potential approach, combined with sliding-mode control for gradient climbing [18,19], and kinematic control

* Corresponding author. Tel.: +61 02404409208.
*E-mail addresses:* almat1712@yahoo.com (A.S. Matveev), z3184703@student.unsw.edu.au, wc42888@hotmail.com (C. Wang), a.savkin@unsw.edu.au (A.V. Savkin).

0921-8890/$ – see front matter © 2012 Elsevier B.V. All rights reserved.
doi:10.1016/j.robot.2012.02.006

based on polar coordinates and Lyapunov-like analysis [20]. Up to now, fully actuated robots were mostly studied in this area, the obstacles were interpreted as rigid bodies of the simplest shapes (e.g., discs [19,20] or polygons [18,21]), the sensory data were assumed to be enough to determine the location of obstacle characteristic points concerned with its global geometry (e.g., the disc center [19,20] or angularly most distant polygon vertex [21]) and to provide access to its full velocity [19,21,20]. Furthermore, rigorous justification of the global convergence of the proposed algorithm is rarely encountered.

In this paper, the problem of reactive navigation is addressed for a robot described by the standard model of the Dubins car type [22], i.e. a nonholonomic under-actuated vehicle moving with a constant speed along planar paths of bounded curvature without reversing direction. This model describes many mechanical systems such as wheeled robots, UAVs, UUV's, missiles, etc.; see e.g. [23,24] and references therein. The robot is strongly perceptually deficient, may observe only a small part of the obstacle, may not distinguish between its points, and so may be unable to estimate many of its parameters, like size, center, edge, full velocity, etc. It has access only to the distance to the nearest obstacle within the sensor range, the time derivative of this measurement, and the angle-of-sight at the target.

Unlike the overwhelming majority of the previous works, the obstacles are not assumed to be rigid or even solid. They are continuums of arbitrary and time-varying shapes that may rotate, twist, wring, skew, wriggle, or be deformed in any other way. This, for example, covers scenarios with reconfigurable rigid obstacles, rigid obstacles with large moving parts, forbidden zones between moving obstacles, like inter-vehicle those in a dense platoon, flexible underwater obstacles, like fishing nets, schools of big fish, bunches of cables, etc., virtual obstacles, like areas corrupted with hazardous chemicals, vapor, radiation, high turbulence etc. or on-line estimated areas of operation of a hostile agent.

Our proposed navigation strategy consists in properly switching between moves to the target in straight lines, when possible, and sliding-mode based bypassing enroute obstacles at a pre-specified distance. When used in isolation, the controller governing the second of these maneuvers solves the problem of patrolling the border of a moving domain with a given safety margin based on only the distance to the border. So it can be used for pure border or perimeter surveillance, which is of independent self-interest. Unlike the previous research in the area, where only static domains were examined and the focus was on multiple vehicle scenario (see e.g. [25]), we solve the problem of patrolling the moving and deforming border and consider a single robot scenario.

When applied to border patrol problems, the proposed controller needs sensors with only a bounded range, which should exceed the safety margin. (This tacitly assumes that initially the border is sensible.) If the sensor range is large enough, we show that the basin of convergence of the closed-loop system is not local and so this controller is suitable for non-local navigation of the robot at the required distance to the moving domain based on range-only measurements. In some cases (e.g., for several scenarios with convex rigid moving domains), the convergence holds from any remote initial location of the robot.

The last feature is of self-interest since the extensive literature on navigation and guidance mostly assumes that the robot has access to both the line-of-sight angle (bearing) and the distance between the robot and the target (range). There is also a relatively large body of research that deals with bearing-only measurements [26,27]. At the same time, only few publications address guidance towards an unpredictable target on the basis of range-only measurements. However, this is of interest in many areas, e.g., wireless networks, unmanned vehicles, surveillance services etc. [28,29] since many sensors typical for these areas, like sonar or range-only radars, provide only the relative distance between the pursuer and the target via, e.g., measurement of the time-of-flight of an acoustics pulse [29] or the strength of the signal radiated by the target [30]. By the best of the authors knowledge, the mathematically rigorous analysis and justification of a range-only navigation law was offered in [31] for a point-wise target moving like a Dubins car. We extend this result on not necessarily point-wise targets subjected to another kinematic constraints.

The navigation strategy considered in this paper develops some ideas set forth in [32]. However in [32], only the case of static rigid domains and relatively sparse scenes with convex obstacles was examined. In this paper, we show that those ideas remain viable for much more general scenarios with moving and deforming domains. We first offer a mathematically rigorous justification of the proposed approach for the problems of patrolling a border of such a domain. This approach originates from the equiangular navigation and guidance law [33,34] and employs sliding-mode regulation; see e.g. [35]. The latter gives rise to concerns about implications of the noises and un-modeled dynamics in practical setting. They are addressed via experimental studies and extensive computer simulations in the second part of the paper, where border patrolling is used as a part of an integrated navigation strategy to safely guide the robot to the target through an environment cluttered with moving non-convex obstacles. The applicability of the proposed strategy is demonstrated via experiments with real robots and extensive computer simulations. In doing so, its performance has been compared with that of the velocity obstacle approach [7,4] and found to be better under certain circumstances.

The remainder of the paper is organized as follows. Section 2 describes the problem of border patrol, whereas Section 4 discusses the main assumptions. Section 3 introduces the navigation law for border patrol and offers its informal discussion, whereas Section 5 presents the main theoretical results of the paper, which are concerned with convergence and performance of this law. Section 6 illustrates these results, along with the assumptions and controller parameters requirements, via their specification in five particular scenarios. The first three of them deal with patrol of the boundary of an arbitrarily shaped rigid body that is steady, or moves with an unknown constant velocity, or undergoes a translational motion with unknown and time-varying velocity and acceleration, respectively. The fourth scenario is about escorting a convoy of several vehicles by an under-actuated robot, whereas the fifth one deals with escort of a single bulky cigar-shaped vehicle. Section 7 introduces the algorithm for guidance towards a target in dynamic environments. The related computer simulations and experimental studies are discussed in Sections 8 and 9, respectively. Section 10 offers brief conclusions.

## 2. System description and the border patrolling problem

We consider a planar under-actuated nonholonomic mobile robot of the Dubins car type [22]. It travels in the given plane with a constant speed $v$ and is controlled by the angular velocity $u$ limited by a given constant $\overline{u}$. In the two-dimensional space, the position of the robot is given by the abscissa $x$ and ordinate $y$ of its characteristic point[1] in the world frame, whereas its orientation is described by the angle $\theta$ from the abscissa axis to the robot centerline; see Fig. 1(a). The kinematics of such robots are classically described by the following equations

$$\begin{array}{ll} \dot{x} = v\cos\theta & \\ \dot{y} = v\sin\theta, & \dot{\theta} = u \in [-\overline{u}, \overline{u}], \\ x(0) = x_0 & \\ y(0) = y_0, & \theta(0) = \theta_0. \end{array} \tag{1}$$

[1] For example, the middle of the rear axle for a four wheeled robot.

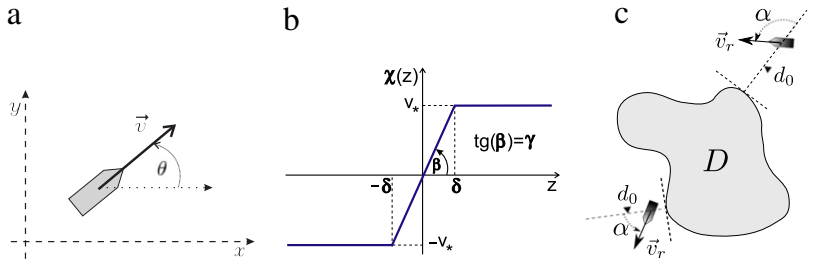


**Fig. 1.** (a) Planar vehicle. (b) Linear function with saturation. (c) Illustration of the navigation law.

In the literature, this model is applied to many mechanical systems such as wheeled robots, UAV's, missiles and autonomous underwater vehicles, which in certain circumstances, have similar governing differential equations; see e.g. [23,36,24] and references therein. These equations capture the capability of the vehicle to travel with the given speed in the forward direction along planar curves whose curvature radius exceeds a given threshold. In the case at hand, this minimal turning radius equals

$$R = v/\bar{u}. \tag{2}$$

Apart from the vehicle, there is an unknown moving domain $D = D(t)$ in the plane. This domain is not necessarily a rigid body: it may perpetually change the shape and undergo any displacements and deformations, including stretches, bends, twists, relative motions of one parts with respect to the others, etc. We do not limit ourselves to a particular type of the domain kinematics and do not specify whether the body $D$ is a rigid, elastic, or plastic solid or a fluid, etc. Moreover, the domain $D$ may represent a virtual structure that obeys no laws governing physical continuums.[2]

To cover a larger range of scenarios, we consider a perceptually deficient robot: it has access only to the current distance $d(t)$ to the current border $\partial D(t)$ and the rate $\dot{d}(t)$ at which this measurement evolves over time. The distance to the moving and deforming domain $D(t)$ is given by $d(t) := \mathbf{dist}_{D(t)}[\boldsymbol{r}(t)]$, where $\boldsymbol{r}(t) := [x(t), y(t)]^\top$ is the vector of the vehicle's Cartesian coordinates,

$$\mathbf{dist}_D(\boldsymbol{r}) := \min_{\boldsymbol{r}' \in D} \|\boldsymbol{r} - \boldsymbol{r}'\|$$

and $\|\cdot\|$ denotes the standard Euclidean norm. This min is achieved if $D$ is closed, which is assumed for $D := D(t)$.

The objective is to design a navigation and guidance law that allows the robot to advance on the a priori unknown moving domain $D(t)$ and then to patrol its border $\partial D(t)$ at the pre-specified distance $d_0$ from it and at the given speed $v$. In doing so, a prescribed safety margin $d_{safe} \in (0, d_0)$ should always be respected: $d(t) \geq d_{safe}\ \forall t$. In some applications, the vehicle should also constantly overtake the nearest boundary point so that the full scan of the border is unavoidably completed in due time. This will be referred to as the *full scan* border patrolling.

We first derive a solution for the border patrolling problem. Then we use this solution as a part of a navigation strategy that drives the robot to a given target while avoiding en-route moving obstacles with a pre-specified safety margin.

The border patrolling problem, as is stated above, in fact consists of two parts: advancement to the body and patrolling itself. The first part is basically the problem of target reaching. Whereas most works in the area assume access to the angle-of-sight at the target for solution of this problem, we ensure advancement to the target at the pre-specified distance based on range-only measurements.

[2] For example, $D(t)$ may be the current estimate of the zone where a hostile agent is operating.

## 3. Navigation for border patrolling

We examine the following navigation law:

$$u(t) = \bar{u} \cdot \mathrm{sgn}\{\dot{d}(t) + \chi[d(t) - d_0]\}, \quad \text{where} \tag{3}$$

$$\chi(z) := \begin{cases} \gamma z & \text{if } |z| \leq \delta \\ v_* \mathrm{sgn}(z) & \text{if } |z| > \delta \end{cases} \quad (v_* := \gamma\delta) \tag{4}$$

is the linear function with saturation (see Fig. 1(b)) and $\gamma, \delta > 0$ are the controller parameters. We stress that this controller generates only admissible controls $u \in [-\bar{u}, \bar{u}]$.

The idea behind the switching law (3) is based on the expectation, confirmed by rigorous analysis in Section 5, that the major part of the robot trajectory corresponds to sliding motion along the switching surface $\dot{d} + \chi(d - d_0) = 0$. To illustrate the geometrical meaning of this equation, we assume that the body $D$ is rigid for simplicity. Then $|\dot{d}| \leq v_r$, where $v_r$ is the speed of the vehicle in the coordinate frame attached to the body. So for the sliding mode to be realistic, the values of $\chi(\cdot)$ should not exceed $v_r$, i.e., $v_* \leq v_r$ in (4). This is ensured by proper tuning of the controller parameters based on analysis of $v_r$, whose detailed discussions will be offered in Sections 5 and 4, respectively. Under the above condition, the angle $\alpha$ subtended by the normal to the body boundary and the vector of the relative velocity $\vec{v}_r$ of the vehicle (see Fig. 1(c)) obeys the equation $\alpha = \arccos[-v_r^{-1}\chi(d - d_0)]$ in sliding mode. According to this equation, this angle is obtuse for $d > d_0$ and acute for $d < d_0$, and thus the vehicle is driven to the required distance $d_0$ in any case.

In the instance of the steady body, the angle $\alpha$ is maintained constant $\alpha = \arccos[\pm v_*/v]$ in the saturation mode, i.e., when the vehicle is far enough from the body $|d - d_0| > \delta$. The geometry of motion with a constant angle between the heading and the direction to the steady target (with negligible size) is described by the so-called equiangular spiral; see e.g., [37]. This pattern of target reaching was discovered in, e.g., insects flying towards a candle and peregrine falcons plummeting towards their preys [38,39]. Inspired by this animal behavior, the equiangular navigation and guidance law $\alpha = \text{const}$ for reaching a steady point-wise target was proposed and studied in [34,33]. In this paper, the applicability of this law is justified for the general case of moving and deforming domains of substantial sizes.

As the vehicle approaches the desired distance $|d - d_0| \leq \delta$, the linear mode of the controller (3), (4) is activated, where $\alpha = \arccos[-(\gamma/v_r)\gamma(d - d_0)]$. Hence for $d = d_0$, the heading is directed parallel to the body boundary $\alpha = \pi/2$, thus driving the robot along the $d_0$-equidistant curve. The speed of 'descent' to this curve $\dot{d}$ is proportional $\dot{d} = -\gamma(d - d_0)$ to the distance $d - d_0$ to it, which is similar to some biologically inspired landing strategies of fixed-wing aircrafts [40, Section X.C].

Practical implementation of the proposed control law requires range-only measurements, including access to the derivative $\dot{d}$. If it is not directly measured, e.g., by the use of the Doppler effect, numerical differentiation of $d$ may be employed. Estimation of derivatives from noise corrupted data is a well-established

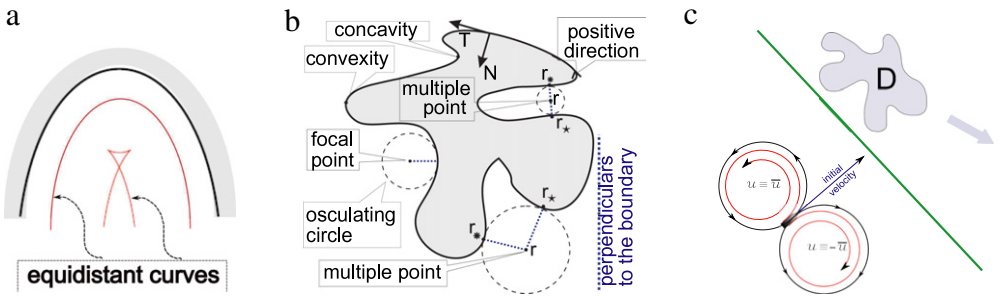


**Fig. 2.** (a) Singularities of equidistant curves. (b) Various types of boundary. (c) Initial circles, points.

discipline, which offers a variety of approaches. Apart from classic numerical differentiation, they include approximation of the transfer function of the ideal differentiator, optimal differentiation based on stochastic models, observers with sliding modes and large gains, difference methods, approximation and Tikhonov regularization, etc. (see e.g., [41,42] for recent surveys). The implications of the numerical differentiation errors will be addressed in Sections 8 and 9 by means of computer simulations and experimental studies. The problem of chattering, which often accompanies the use of switching controllers like (3), will be addressed in Section 9 via experimental studies as well.

For the control objective to be achievable, the vehicle should be capable of tracking the $d_0$-equidistant curve of the body boundary. However this is impossible irrespective of the vehicle's capabilities if this curve contains cusp singularities, so far as any path of the unicycle (1) is everywhere smooth. Such singularities are typically born whenever the boundary contains concavities and the required distance $d_0$ exceeds a critical value, which is equal the minimal curvature radius of the concavity parts of the boundary [43]; see Fig. 2(a). In this case, the objective of maintaining the distance $d = d_0$ cannot be achieved by any means and should be replaced by a realistic one, e.g., to follow a non-equidistant path that smoothly connects the regular parts of the equidistant curve. Due to the paper length limit, we consider the related developments, including path planning, as a topic of future research and assume in this paper that if the body boundary contains concavities, the required distance $d_0$ is so small that the related equidistant curve is smooth. This also ensures uniqueness of the minimum-distance point [37].

The preliminary analysis in the previous paragraph tacitly assumed that the body is rigid and steady. In this case, the global convergence of the controller (3), (4) was theoretically justified in [32]. In Section 5, we extend these results on a much wider class of moving and deforming domains. To this end, we first establish conditions necessary for the control objective to be achievable in this general case (Lemma 4.1). Assuming that these unavoidable conditions do hold in a slightly enhanced form (Assumption 5), we show that this is enough for the controller (3), (4) to ensure the local stability of the output $d$ near $d_0$ (Lemma 5.1). Global convergence is established in Theorem 1 at the expense of extending the above conditions from the vicinity of the equidistant curve to the estimated area of the transient localization.

## 4. Main assumptions

To qualitatively describe the properties of the moving continuum $D(t)$, we use the Lagrangian formalism: we introduce a *reference configuration* $D_* \subset \mathbb{R}^2$ of the body and the *configuration map* $\Phi(\cdot, t) : \mathbb{R}^2 \to \mathbb{R}^2$ that transforms $D_*$ into the current configuration $D(t) = \Phi[D_*, t]$. We limit ourselves by only few conventions typical for the continuum mechanics and listed in the following.

**Assumption 1.** The reference domain $D_*$ is compact and has a smooth boundary $\partial D_*$. The configuration map $\Phi(\cdot, t)$ is defined on an open neighborhood of $D_*$ and is smooth, the determinant of its Jacobian matrix is everywhere positive $\det \Phi'_{\boldsymbol{r}} > 0$, and $\Phi(\boldsymbol{r}_1, t) \neq \Phi(\boldsymbol{r}_2, t)$ whenever $\boldsymbol{r}_1 \neq \boldsymbol{r}_2$.

These assumptions imply that the topological properties of $D(t)$ do not change as time progresses (the body $D(t)$ remains homeomorphic to itself), e.g., the body does not split into separate parts or intersect with itself, etc.[3] Furthermore, the boundary $\partial D(t)$ is smooth at any time.

To proceed, we need some notations, which partly refer to the Eulerian formalism in description of the body motion:

- $\Phi^{-1}(\cdot, t)$ — the inverse map;
- $\vec{V}(\boldsymbol{r}, t) := \Phi'_t[\Phi^{-1}(\boldsymbol{r}, t)]$ — the velocity vector-field;
- $\vec{A}(\boldsymbol{r}, t) := \Phi''_{tt}[\Phi^{-1}(\boldsymbol{r}, t)]$ — the acceleration vector-field;
- $\vec{V}'_{\boldsymbol{r}}[\boldsymbol{r}, t]$ — the spatial velocity gradient tensor;
- $\mathscr{E} := \frac{1}{2}[\vec{V}'_{\boldsymbol{r}}[\boldsymbol{r}, t] + \vec{V}'_{\boldsymbol{r}}[\boldsymbol{r}, t]^\top]$ — the strain rate tensor;
- $\omega = \omega(\boldsymbol{r}, t)$ — the vorticity, or angular velocity of the rigid-body-rotation i.e., $\begin{pmatrix} 0 & \omega \\ -\omega & 0 \end{pmatrix} = \frac{1}{2}[\vec{V}'_{\boldsymbol{r}} - \vec{V}'^{\top}_{\boldsymbol{r}}]$;
- $\langle \cdot ; \cdot \rangle$ — the standard inner product;
- $\vec{T}(\boldsymbol{r}, t), \vec{N}(\boldsymbol{r}, t)$ — the Frenet frame of $\partial D(t)$ at $\boldsymbol{r} \in \partial D(t)$; the domain $D(t)$ is to the left to the tangent vector $\vec{T}$, the normal vector $\vec{N}$ is directed inwards $D(t)$;
- $W_{T,t}(\boldsymbol{r}, t) := \langle \vec{W}(\boldsymbol{r}, t); \vec{T}(\boldsymbol{r}, t) \rangle$ — the tangential component of the vector-field $\vec{W}$ at the point $\boldsymbol{r} \in \partial D(t)$;
- $W_{N,t}(\boldsymbol{r}, t)$ — the normal component at the point $\boldsymbol{r} \in \partial D(t)$;
- $\kappa(\boldsymbol{r}, t)$ — the signed curvature of $\partial D(t)$ at the point $\boldsymbol{r}$;
- $\sigma[\boldsymbol{r}, t] := \langle \mathscr{E}\vec{T}; \vec{N} \rangle + \omega = \langle \vec{V}'_{\boldsymbol{r}}\vec{T}; \vec{N} \rangle$ — the normal component of the velocity rate-of-change under an infinitesimally small shift along the boundary $\partial D(t)$;
- $\boldsymbol{r}(t)$ — the current position of the vehicle;
- $\boldsymbol{r}_*(t)$ — the point of $\partial D(t)$ nearest to $\boldsymbol{r}(t)$.

The signed curvature $\kappa$ assumes positive and negative values on the convex and concave parts of $\partial D(t)$, respectively, so that the Frenet–Serret equations are satisfied, i.e.,

$$\frac{\mathbf{d}\vec{T}}{\mathbf{d}s} = \kappa\vec{N}, \qquad \frac{\mathbf{d}\vec{N}}{\mathbf{d}s} = -\kappa\vec{T}, \tag{5}$$

where $s$ is the natural parameter on $\partial D(t)$; see Fig. 2(a).

We also recall the following useful relations [44, Chapter 4]

$$\vec{A} = \vec{V}'_{\boldsymbol{r}}\vec{V} + \vec{V}'_t, \qquad \Phi''_{\boldsymbol{r}t} = \vec{V}'_{\boldsymbol{r}}[\Phi, t]\Phi'_{\boldsymbol{r}}. \tag{6}$$

The second technical assumption serves asymptotic (as $t \to \infty$) analysis of the closed-loop system.

[3] This does hold for many solids but may be a restriction for, e.g., fluids or virtual bodies.

**Assumption 2.** The scalars $V_N[\boldsymbol{r}, t]$, $V_T[\boldsymbol{r}, t]$, $A_N[\boldsymbol{r}, t]$, $\sigma[\boldsymbol{r}, t]$, $\kappa[\boldsymbol{r}, t]$ remain bounded as $\boldsymbol{r} \in \partial D(t)$ and $t \to \infty$.

It is worth noting that these quantities are bounded over $\boldsymbol{r} \in \partial D(t)$ and $t$ within any finite time horizon since all of them, along with $\Phi(\boldsymbol{r}, t)$, continuously depend on $\boldsymbol{r}$ and $t$, and the reference domain $D_*$ is compact by Assumption 1.

Due to restricted maneuverability, the robot is not always capable of border patrolling. Briefly, the $d_0$-equidistant curve to be traced should not move too fast and be sharply contorted due to the limited turning radius (2). The following discussion details these requirements and provides an evidence that the main of them are nearly unavoidable.

**Definition 1.** A point $\boldsymbol{r} \notin D$ is said to be *multiple* (for $D$) if there exist two different *minimum-distance* points $\boldsymbol{r}_*, \boldsymbol{r}_\star \in D$, i.e., such that $\mathbf{dist}_D(\boldsymbol{r}) = \|\boldsymbol{r} - \boldsymbol{r}_*\| = \|\boldsymbol{r} - \boldsymbol{r}_\star\|$, and *focal* if there exists a minimum-distance point $\boldsymbol{r}_* \in D$ such that $1 + \mathbf{dist}_D(\boldsymbol{r})\kappa = 0$, where $\kappa$ is the curvature of $\partial D$ at $\boldsymbol{r}_*$.

These notions are illustrated in Fig. 2(b).

As is shown in [32], the following assumption is nearly unavoidable in the case of the static $D(t) \equiv D$ domain.

**Assumption 3.** There are neither multiple nor focal points at the $d_0$-equidistant curve of the domain $D(t)$.

For any point $\boldsymbol{r}$ on the equidistant curve, there are no focal points between $\boldsymbol{r}$ and the nearest point $\boldsymbol{r}_* \in D(t)$ [45, Chapter 16]. Assumption 3 excludes the marginal case where the end $\boldsymbol{r}$ of the segment $[\boldsymbol{r}, \boldsymbol{r}_*]$ is focal. Furthermore, this assumption implies that $1 + \varkappa d_0 > 0$ on the $d_0$-equidistant curve. Now we require that this remains true as $t \to \infty$.

**Assumption 4.** The following relation holds:

$$\lim_{t\to\infty} \inf_{\boldsymbol{r}\in\partial D(t):\kappa[\boldsymbol{r},t]<0} (1 + d_0\kappa[\boldsymbol{r}, t]) > 0. \tag{7}$$

This necessarily holds if either $D(t)$ is convex or $d_0$ is small enough [45, Chapter 16]. The following lemma discloses conditions necessary for the control objective to be realistic.

**Lemma 4.1.** *Let the vehicle travel so that $d(t) \equiv d_0$. For any time $t$, the parameters of the domain motion at the point $[\boldsymbol{r}_*(t), t]$ satisfy the following relations:*

$$|V_N| \le v, \qquad \overline{u} \ge \frac{|\mathscr{A}|}{\sqrt{v^2 - V_N^2}}, \quad \textit{where}$$

$$\mathscr{A} = \mathscr{A}(\boldsymbol{r}_*, t, d_0) := A_N + \frac{2\sigma\xi + \kappa\xi^2 - d_0\sigma^2}{1 + \kappa d_0} \quad \textit{and}$$

$$\xi := -V_T \pm \sqrt{v^2 - V_N^2}. \tag{8}$$

*If the vehicle overtakes the nearest boundary point, then*

$$\sqrt{v^2 - V_N^2} \ge \pm(V_T + d_0\sigma). \tag{9}$$

*In (8) and (9), the sign $+$ is taken if the vehicle moves so that the domain is to the left, and $-$ is taken otherwise.*

The proofs of all theoretical claims are given in Appendix.

Thus conditions (8) must be satisfied, otherwise the control objective can be achieved by no means. Since the nearest boundary point $\boldsymbol{r}_*(t)$ is not known in advance, it is reasonable to require that (8) holds for all boundary points at any time. The next assumption enhances a bit this by substituting the uniformly strict inequality in place of the non-strict one.

**Assumption 5.** There exist $\lambda_v, \lambda_a \in (0, 1)$ such that

$$|V_N| \le \lambda_v v, \qquad \frac{|\mathscr{A}|}{\sqrt{v^2 - V_N^2}} \le \lambda_a \overline{u} \tag{10}$$

at any time $t$, point $\boldsymbol{r}_* \in \partial D(t)$, and with both signs $\pm$.

For any finite time horizon, such $\lambda_v, \lambda_a$ exist if and only if the left-hand sides from (10) are strictly less than $v$ and $\overline{u}$, respectively, for all concerned $\boldsymbol{r}_*$ and $t$. By introduction of $\lambda_v, \lambda_a$, we ensure that the discrepancies between right- and left-hand sides do not vanish as $t \to \infty$.

The strict inequalities contained in (10) allow not only to maintain the distance to the domain $\dot{d} = 0$ but also to make it both descending $\dot{d} < 0$ and ascending $\dot{d} > 0$. In other words, they in fact guarantee that the output $d$ is locally controllable. As will be shown, the above assumptions are enough for local stability of the closed-loop system in a vicinity of the desired equidistant trajectory. To establish non-local convergence to this trajectory, we need to ensure controllability during the transient. To this end, we introduce two definitions.

**Definition 2.** An interval $[d_-, d_+]$ is said to be *regular* if there exist $\lambda_v, \lambda_a \in (0, 1)$ such that Assumptions 3–5 hold with $d_0$ replaced $d_0 := d$ by any $d$ from this interval.

Since in (8), $\mathscr{A}$ is the (first degree)/(first degree) rational function in $d_0$, simple calculus show that it suffices to check Assumption 5 only for $d = d_-, d_+$. Similarly Assumption 4 holds for all $d \in [d_-, d_+]$ if and only if

$$\lim_{t\to\infty} \inf_{\boldsymbol{r}\in\partial D(t):\kappa[\boldsymbol{r},t]<0} (1 + d_+\kappa[\boldsymbol{r}, t]) > 0.$$

**Remark 1.** Any interval $[d_-, d_+]$, where $d_-, d_+$ are close enough to $d_0$, is regular due to uniform continuity of the concerned expressions from (7) and (10) in $d_0$.

We however need more: this interval can be expanded to include all distances $d(t)$ that may be encountered during the transient. To flesh out this, we introduce the following.

**Definition 3.** The $\pm$-*initial circle* is the path of the robot driven by the maximal actuation $u \equiv \pm\overline{u}$ from its initial position; the corresponding robot motion during the first one and a half full turn over the initial circle is said to be $\pm$-*initial* (see Fig. 2(c)). The distance from the robot to $D(t)$ observed within any initial motion is said to be *launching*.

Now we summarize the above discussion by imposing the cumulative assumption, which covers Assumptions 3–5.

**Assumption 6.** Let $\mathfrak{D}$ be the set composed of all launching distances $d$ and $d := d_0$, and $d_- := \min_{d\in\mathfrak{D}} d$, $d_+ := \max_{d\in\mathfrak{D}} d$. The interval $[d_-, d_+]$ is regular and $d_- > d_{\text{safe}}$.

The last requirement ensures that any initial motion (which lasts $\frac{3\pi}{\overline{u}}$ time units) does not involve collisions with $D(t)$. The last assumption enhances this.

**Assumption 7.** During the first $\frac{3\pi}{\overline{u}}$ time units, the body $D(t)$ and the union of the initial circles remain in disjoint steady half-planes; see Fig. 2(c).

In other words, the robot starts far enough from the domain.

## 5. Main results concerning the border patrolling problem

To properly tune the parameters of the controller (3), (4), two real parameters $\eta_v > 0$, $\eta_a > 0$ should first be picked such that

$$\lambda_v + \eta_v < 1, \qquad \lambda_a + \eta_a < 1, \tag{11}$$

where $\lambda_v, \lambda_a < 1$ are the parameters associated with the regular interval at hand by Definition 2. Furthermore, we note that for any choice of the sign in $\pm$, the function

$$\Omega(\boldsymbol{r}_*, t, d, z) := \frac{A_N + \frac{2\sigma\bar{\xi}+\kappa\bar{\xi}^2-d\sigma^2}{1+\kappa d}}{\sqrt{v^2-(V_N+z)^2}},$$

$$\text{where} \quad \bar{\xi} := -V_T \pm \sqrt{v^2-(V_N+z)^2} \tag{12}$$

is continuous in $z \approx 0$ uniformly over $\boldsymbol{r}_* \in \partial D(t), t \geq 0, d \in [d_-, d_+]$ and for $z := 0$, its absolute value equals the left-hand side of the second inequality from (10). Hence there exists $z_* > 0$ such that for above $\boldsymbol{r}_*, t, d$,

$$|\Omega(\boldsymbol{r}_*, t, d, z)| < (\lambda_a + \eta_a)\bar{u} \quad \forall z \in [-z_*, z_*]. \tag{13}$$

Now we are in a position to state the first result concerning the border patrolling problem.

**Theorem 1.** *Let Assumptions 1, 2, 6 and 7 be satisfied and the robot be driven by the navigation rule (3), (4), where the parameters $\gamma > 0$ and $\delta > 0$ are chosen so that*

$$\begin{aligned} &v_* = \gamma\delta \leq \min\{\eta_v v, z_*\}, \\ &\gamma v_* < v\bar{u}[1-(\lambda_a+\eta_a)]\sqrt{1-(\lambda_v+\eta_v)^2}. \end{aligned} \tag{14}$$

*Then the following statements hold:*

- **i.** *The navigation law (3) asymptotically drives the robot at the desired distance to D, i.e., $d(t) \xrightarrow{t\to\infty} d_0, \dot{d}(t) \xrightarrow{t\to\infty} 0$.*
- **ii.** *The safety margin is always respected: $d(t) \geq d_{safe}\ \forall t$.*
- **iii.** *The motion splits into the transient and sliding motion.*
  - (a) *The transient holds while $S := \dot{d} + \chi(d-d_0) \neq 0$, necessarily terminates, and lasts no longer than $\frac{3\pi}{\bar{u}}$ time units; during this phase, the vehicle is driven by a constant control $u \equiv \pm\bar{u}$ along an initial circle.*
  - (b) *After the transient, a sliding motion [35] over the surface $S = 0$ is commenced and afterward, maintained, which results in monotonic and exponentially fast convergence of the robot to the desired distance $d_0$ to the domain.*
  - (c) *During the sliding motion, the angle $\alpha(t)$ between the robot velocity $\vec{v}(t)$ and the tangent vector $\vec{T}[\boldsymbol{r}_*(t), t]$ is constantly acute, i.e., the robot encircles the domain $D(t)$ so that it is to the left.*

The choice of the controller parameters $\delta, \gamma$ from (4) recommended by this theorem is always possible under the assumptions made. Indeed, since $\lambda_v, \lambda_a < 1$ thanks to Assumption 5, inequalities (11) can be satisfied by picking $\eta_v \in (0, 1-\lambda_v)$, $\eta_a \in (0, 1-\lambda_a)$. After this, (13) can be ensured by picking small enough $z_*$, as has been shown. It remains to choose $v_*$ and $\gamma$ small enough to ensure (14) and put $\delta := \gamma^{-1}v_*$.

**Remark 2.** It follows from **iii** that during the entire maneuver, the distance from the robot to the moving body remains in the interval $[d_-, d_+]$ from Assumption 6. So the sensor range may be upper limited by $d_+$: the navigation law (3) can be implemented and achieves the control objective even if the sensor provides the distance $d$ only when $d \leq d_+$.

**Remark 3.** Theorem 1 remains true for the navigation law (3) with the reversed sign

$$u(t) = -\bar{u} \cdot \operatorname{sgn}\{\dot{d}(t) + \chi[d(t)-d_0]\} \tag{15}$$

provided that in iii.(c), "acute" and "to the left" are replaced by "obtuse" and "to the right", respectively.

The following lemma shows that Assumptions 6 and 7 are responsible only for transition of the robot from a remote location to motion along the required equidistant curve based on range-only measurements. If the robot is initially close to this curve and nearly tracks it, this navigation law ensures stable maintenance of the required distance under much milder and partly unavoidable Assumptions 1–5.

**Lemma 5.1.** *Suppose that only Assumptions 1–5 are true and the controller parameters are chosen so that (14) is satisfied with $\lambda_v, \lambda_a$ and $z_*$ taken from (10) and (13), where only $d = d_0$ is considered. Then the following claims hold:*

- **i.** *For proper initial states, the navigation law (3) does generate the desired motion: whenever at some time instant $d = d_0, \dot{d} = 0$ and the angle $\alpha$ from* iii.(c) *is acute, these features remain true afterward.*
- **ii.** *This motion is locally stable: for any $\varepsilon_0 > 0$ there exists $c = c(\varepsilon_0) > 0$ and $\tau = \tau(\varepsilon_0) > 0$ such that*

$$\boxed{|d(t_0)-d_0| < c \ |\dot{d}(t_0)| < c, \ |\alpha(t_0)| < \frac{\pi}{2}}$$

$$\Downarrow \qquad \Downarrow$$

$$\overbrace{\begin{matrix}|d(t)-d_0| < \varepsilon_0 \\ |\dot{d}(t)| < \varepsilon_0 \\ t \geq t_0\end{matrix}} \quad \overbrace{\begin{matrix}d(t) = d_0 \\ \dot{d} = 0 \\ \forall t \geq t_0 + \tau\end{matrix}} \tag{16}$$

*where $\tau(\varepsilon_0) \to 0$ as $\varepsilon_0 \to 0$.*

By the first entailment, local stability requires sensors that give access to $d$ only at the distances $d \leq d_0 + \varepsilon_0$, where $\varepsilon_0 > 0$ may be arbitrarily small.

When dealing with non-local convergence, requirements to the vehicle's initial state and the desired distance (like Assumptions 6 and 7) are unavoidable since the navigation law (3) is unable to ensure global convergence even in the simplest case of a point-wise steady domain [32].

Lemma 5.1 remains true for the navigation law with the reversed sign discussed in Remark 3 provided that in **i** of the lemma, "acute" and replaced by "obtuse" and in (16), $|\alpha| < \frac{\pi}{2}$ is reversed into $|\alpha| > \frac{\pi}{2}$.

The next remark addresses the full scan patrolling. In the necessary condition (9) for such a mission to be realistic, the boundary point and the sign are not known in advance. So it is natural to require that this condition be satisfied for all boundary points and with any sign:

$$\sqrt{v^2-V_N^2} \geq |V_T + d_0\sigma| \quad \forall \boldsymbol{r}_* \in \partial D(t), t. \tag{17}$$

Since $V_N^2 + V_T^2 = \|\vec{V}\|^2$, this can be shaped into

$$v^2 \geq \|\vec{V}\|^2 + 2V_T d_0\sigma + d_0^2\sigma^2 \quad \forall \boldsymbol{r}_* \in \partial D(t), t.$$

**Remark 4.** Suppose that the hypotheses of Theorem 1 are true and the condition (17) holds with the strict inequality sign and uniformly over the infinite time horizon:

$$\inf_{\boldsymbol{r}_* \in \partial D(t), t \geq 0} \left[\sqrt{v^2-V_N^2} - |V_T + d_0\sigma|\right] > 0.$$

Then since some time instant, the robot constantly overtakes the nearest boundary point. Moreover, its speed exceeds that of this point by a positive time-invariant constant.

Our last remark concerns the choice of the parameter $z_* > 0$, which requires to analyze (13). Since this analysis usually follows

that of 'almost necessary' conditions (10), it is worth of noting that (13) is identical to the second condition in (10) written for $\lambda_a := \lambda_a + \eta_a$ and $v := \sqrt{v^2 - 2V_N z - z^2}$. So it suffices to pick $z_*$ so that the latter condition is satisfied with any $z \in [-z_*, z_*]$ and feasible $V_N$. Moreover, since $|V_N| \leq v$ by (10), it suffices to ensure that this condition holds for all speed values from $[\sqrt{v^2 - 2vz_* - z_*^2}, \sqrt{v^2 + 2vz_* - z_*^2}]$ or even from the larger and simpler interval $[v - \frac{z_*}{\sqrt{2}-1}, v + z_*]$.[4] This may be easier than the direct analysis of (13) though provides less conservative conditions.

## 6. Illustrative examples of border patrolling

The foregoing assumptions and parameter requirements employ some knowledge about the body $D(t)$ that is rarely available in the requested details. Typically only some qualitative features and estimates are known a priori, which determine a whole class of body motions. For the practical design, this means the need to extend the assumptions and requirements on any motion from this class. Now we offer illustrative examples of such extensions. For rigid bodies, $D$ (without $(t)$) will stand for the snapshot of the body at an arbitrary time instant; the boundary $\partial D$ is assumed to be smooth in the examples 6.1–6.3.

### 6.1. Steady rigid body

The velocity $\vec{V}$ and acceleration $\vec{A}$ vector-fields are identically zero. As can be easily seen by inspection, Assumptions 1–5 mean that the following properties hold:

**(p)** there are no multiple points at the distance $d_0$ from $D$;

$$R_\varkappa(\boldsymbol{r}_*, d_0) := \frac{1}{|\kappa(\boldsymbol{r}_*)|} + d_0 \mathrm{sgn}\kappa(\boldsymbol{r}_*) > R \quad \forall \boldsymbol{r}_* \in \partial D. \tag{18}$$

Here $R$ is the minimal turning radius (2) of the robot and $R_\varkappa(\boldsymbol{r}, d_0)$ is the curvature radius of the $d_0$-equidistant curve to be tracked. Inequality (18) means that the robot is capable of tracking this curve, which is an unavoidable requirement. By Lemma 5.1, this is enough for the navigation law (3) to ensure local stability if in (3), $v_*$, $\gamma$ are chosen so that

$$v_* < v, \quad \max_{\boldsymbol{r}_* \in \partial D} \frac{R}{R_\varkappa(\boldsymbol{r}_*, d_0)} + \frac{\gamma v_*}{\overline{u}\sqrt{v^2 - v_*^2}} < 1, \tag{19}$$

which is always possible under the condition (18). For the non-local convergence, Assumptions 6 and 7 are needed. They and (14) mean that the union of the initial circles can be separated from $D$ by a line, **(p)** holds for $d_0 := d : \forall d \in [d_-, d_+]$, and (18), (19) are true with $d_0 := d_-, d_+$, where $d_-$ and $d_+$ are the minimal and maximal distance, respectively, from the points of this union to $D$.

If $\kappa(\boldsymbol{r}_*) \geq 0$ $\forall \boldsymbol{r}_* \in \partial D$ (i.e., if $D$ is convex), (18) and (19) are true for all large enough $d_0$ (provided that small enough $v_*$ is taken). This implies that the controller at hand navigates the robot to the domain from any remote enough initial location based on range-only measurements.

Up to now, we tacitly assumed that $D$ is known. Now let only the lower estimates of the boundary curvature radius $R_\kappa(\boldsymbol{r}_*) = |\kappa(\boldsymbol{r})|^{-1}$ be known, which are separate for convex $R_\kappa(\boldsymbol{r}_*) \geq R_+$ $\forall \boldsymbol{r}_* \in \partial D : \kappa(\boldsymbol{r}_*) \geq 0$ and concave $R_\kappa(\boldsymbol{r}_*) \geq R_-$ $\forall \boldsymbol{r}_* \in \partial D : \kappa(\boldsymbol{r}_*) \leq 0$ parts of the boundary. Then the focus on the worst case scenario within these bounds yields that (18) should be replaced by $R_\pm > R \mp d_0$ and (19) by $v_* < v$, $\frac{R}{\min\{R_+ + d_0, R_- - d_0\}} + \frac{\gamma v_*}{\overline{u}\sqrt{v^2 - v_*^2}} < 1$. Then the foregoing remains true.

[4] The square roots are well-defined if $z_* \in (0, [\sqrt{2} - 1]v)$.

### 6.2. Rigid body moving with a constant speed $v$ in a priori unknown and fixed direction

Let $\alpha(\boldsymbol{r}_*)$ be the polar angle of $\vec{V}$ in the Frenet frame $\vec{T}(\boldsymbol{r}_*), \vec{N}(\boldsymbol{r}_*)$. Since $\vec{A} \equiv 0, \sigma \equiv 0$, trivial manipulations reduce (10) to the requirement that for all $\boldsymbol{r}_* \in \partial D$,

$$\mu := \frac{v}{V} \geq \lambda_v^{-1} |\sin\alpha(\boldsymbol{r}_*)|,$$

$$\lambda_a^{-1} R \leq R_\kappa(\boldsymbol{r}_*, d_0) \frac{\mu\sqrt{\mu^2 - \sin^2\alpha(\boldsymbol{r}_*)}}{\left(|\cos\alpha(\boldsymbol{r}_*)| + \sqrt{\mu^2 - \sin^2\alpha(\boldsymbol{r}_*)}\right)^2}.$$

Elementary calculus show that the right hand side of the last inequality decreases as $|\cos\alpha(\boldsymbol{r}_*)|$ increases. By putting here the worst velocity scenario (for which $|\cos\alpha(\boldsymbol{r}_*)| = 1$), we see that (18) still holds and for all $\boldsymbol{r}_* \in \partial D$,

$$V \leq \lambda_v v < v, \qquad \frac{(V+v)^2}{R_\varkappa(\boldsymbol{r}_*, d_0)} \leq \lambda_a v \overline{u} < v\overline{u}. \tag{20}$$

Thus Assumptions 1–5 hold for all velocity $\vec{V}$ headings if and only if **(p)** and (18), (20) are true. Lemma 4.1 and the foregoing imply that these requirements are 'almost necessary' for the robot to be capable of the border patrolling irrespective of the direction in which the body moves. By Lemma 5.1, they are simultaneously sufficient for the navigation law (3) to ensure local stability if $\delta$, $\gamma$ in Fig. 1(b) are chosen so that (14) holds, where $\eta_\nu \in (0, 1 - \lambda_\nu)$, $\nu = v, a$ and

$$z_* \leq \min_{\boldsymbol{r}_* \in \partial D} \sqrt{(\lambda_a + \eta_a) v \overline{u} R_\varkappa(\boldsymbol{r}_*, d_0)} - V - v. \tag{21}$$

The expression $\frac{(V+v)^2}{R_\varkappa(\boldsymbol{r}_*, d_0)}$ in (20) is the centrifugal acceleration of the point tracing the $d_0$-equidistant curve at the speed $v$ in the case where the velocity of the nearest boundary point is tangential to the boundary and directed opposite to that of the point; see Fig. 3(a). The expression $v\overline{u}$ gives the maximal linear acceleration of the robot (1). So the second inequality in (20) means that the robot is able to produce accelerations required for the curve tracking in any direction.

Now suppose that Assumption 7 holds. Under the circumstances, Assumption 6 means that **(p)** is valid for $d_0 := d : \forall d \in [d_-, d_+]$, and (18), (20) are true with $d_0 := d_-, d_+$, where $d_-$ and $d_+$ are the minimal and maximal distances, respectively, from the points of the union of the initial circles to the body within the first $\frac{3\pi}{\overline{u}}$ time units of its motion. The parameter $z_*$ involved in the controller design should be taken as the minimum among the right-hand sides of (21) calculated for $d_0 := d_-$ and $d_0 := d_+$, respectively. Under these assumptions, non-local convergence (i.e., the conclusion of Theorem 1) holds. $v_*$ is taken

For convex $D$, the argument similar to that from the previous subsection shows that the convergence holds whenever initially the robot is remote enough from the domain.

Now let $V$ be unknown but can be estimated $V \leq \overline{V}$ by a known constant. It is easy to see that the foregoing remains true if $V$ is formally replaced by $\overline{V}$ everywhere.

### 6.3. Translational motion of a rigid body

Suppose that only upper bounds $V_+ \geq \|\vec{V}(t)\|, A_+ \geq \|\vec{A}(t)\|$ on the body velocity $\vec{V}(t)$ and acceleration $\vec{A}(t)$ are unknown. Since the motion is translational, $\vec{V}(\boldsymbol{r}, t) = \vec{V}(t)$, $\frac{\partial \vec{V}}{\partial \boldsymbol{r}} \equiv 0, \sigma \equiv 0$ and (10) takes the form

$$|V_N| \leq \lambda_v v, \qquad \frac{\left|A_N + \frac{\left(V_T \mp \sqrt{v^2 - V_N^2}\right)^2}{R_\kappa(\boldsymbol{r}_*, d_0)} \mathbf{sgn}\kappa\right|}{\sqrt{v^2 - V_N^2}} \leq \lambda_a \overline{u}.$$

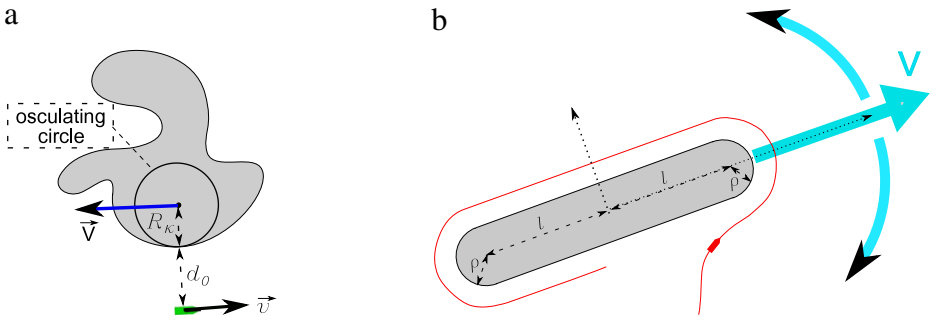


**Fig. 3.** (a) The worst case scenario. (b) Escorting a bulky vehicle.

The first inequality holds for all feasible velocities iff

$$V_+ \le \lambda_v v < v. \tag{22}$$

Given the value of $V_N$, the worst case scenario for the second inequality is attained when $A_N = A_+ \mathbf{sgn}\kappa$ and $V_T = \mp\sqrt{V_+^2 - V_N^2}$. Then this inequality takes the form

$$\frac{A_+}{\sqrt{v^2 - V_N^2}} + \frac{\Psi(|V_N|)}{R_\kappa(\boldsymbol{r}_*, d_0)} \le \lambda_a \bar{u}, \quad \text{where } 0 \le |V_N| \le V_+,$$

$$\Psi(z) := \frac{\left(\sqrt{V_+^2 - z^2} + \sqrt{v^2 - z^2}\right)^2}{\sqrt{v^2 - z^2}}. \tag{23}$$

For $z \in [0, V_+]$, $A := \sqrt{V_+^2 - z^2}$, $B := \sqrt{v^2 - z^2}$, we have

$$\begin{aligned}(v^2 - z^2)\frac{d\Psi}{dz}(z) &= 2(A+B)\left(-\frac{z}{A} - \frac{z}{B}\right)B + (A+B)^2\frac{z}{B} \\ &= (A+B)^2 z\frac{A-2B}{AB} \overset{V_+<v}{<} 0,\end{aligned}$$

i.e., $\Psi(|V_N|)$ decreases as $|V_N|$ increases, whereas the first addend in the left-hand side of the inequality from (23) conversely increases. This complicates analytically finding the maximum of the entire left-hand side.

Anyhow, the second inequality from (10) holds for all feasible scenarios if and only if for all $\boldsymbol{r}_* \in \partial D$,

$$\max_{z\in[0,V_+]}\left[\frac{A_+}{\sqrt{v^2 - z^2}} + \frac{\Psi(z)}{R_\kappa(\boldsymbol{r}_*, d_0)}\right] \le \lambda_a \bar{u} < \bar{u}. \tag{24}$$

By separately maximizing the first and second addend, we see that (24) is implied by the more constructive condition

$$\frac{A_+}{\sqrt{1 - \frac{V_+^2}{v^2}}} + \frac{(V_+ + v)^2}{R_\kappa(\boldsymbol{r}_*, d_0)} \le \lambda_a \bar{u} v < \bar{u} v.$$

Note that for $A_+ := 0$, (22) plus either the last inequality or inequality (24) reduce to (20).

Overall, we see that Assumptions 1–5 hold for all feasible scenarios if and only if **(p)**, (18), (22) and (24) are true. Moreover, these requirements are 'almost necessary' for the robot to be capable of performing the border patrol irrespective of the scenario. By Lemma 5.1, they are simultaneously sufficient for the navigation law (3) to ensure locally stable patrolling if $\delta, \gamma$ in Fig. 1(b) are chosen so that (14) holds, where $\eta_v \in (0, 1-\lambda_v)$, $\nu = v$, $a$ and $z_* \in (0, V_+)$ is chosen so that (24) is true for $V_+ := V_+ + z_*$ and $\lambda_a := \lambda_a + \eta_a$.

Analysis similar to that from the previous subsection shows that for non-local convergence (i.e., for the conclusion of Theorem 1 to be valid) it suffices that Assumption 7 is true, **(p)** is valid for $d_0 := d : \forall d \in [d_-, d_+]$, and (18), (24) are true with $d_0 := d_-, d_+$, where $d_-$ and $d_+$ are the minimal and maximal distances, respectively, from the points of the union of the initial circles to the body within the first $\frac{3\pi}{\bar{u}}$ time units of its motion. The parameter $z_*$ involved in the controller design should be taken as the minimum among the values calculated in accordance with the above recommendations for $d_0 := d_-$ and $d_0 := d_+$, respectively.

For convex $D$, (24) remains true as $d_0$ grows. So the argument similar to that from the previous subsection shows that the convergence holds whenever initially the robot is remote enough from the moving domain.

### 6.4. Escorting a convoy of unicycle-like vehicles

$N$ planar vehicles travel with a constant speed $V$ in a convoy one after another. The first of them acts as leader; every other vehicle traces the path of its predecessor at the distance[5] $\Delta s$ from it. There also is a mobile escort robot. It has to constantly encircle the entire convoy with the margin $d_0$, not intervening between the vehicles; see Fig. 4(a).

The leader motion obeys the unicycle-like equations:

$$\dot{X} = V\cos\alpha, \qquad \dot{Y} = V\sin\alpha, \qquad \dot{\alpha} = \omega. \tag{25}$$

Here $X$ and $Y$ are its abscissa and ordinate, respectively, in the world frame, $\alpha$ gives the orientation of the linear velocity vector, and the angular velocity $\omega$ is time-varying. The escort robot is interpreted as that discussed in Section 2; its governing equations are given by (1).

We assume that any vehicle in the convoy can be approximated by a disc of the radius $\rho$. Correspondingly, the escort robot should be at the distance $d_0$ from the union of $N$ discs, each of the radius $\rho$, whose centers are uniformly distributed over the path $\mathscr{P}|_{t-\tau}^{t}$ tracked by the leader during the last $\tau := (N-1)\Delta s/V$ time units. In this demand, we upgrade '$N$ discs' into 'all discs'; see Fig. 4(b), where the dotted line is the locus of desirable positions of the escort robot and $N = 4$. In other words, we inject more safety by requiring that the convoy is escorted at the distance $d_0$ from the union $D(t)$ of all $\rho$-discs centered at $\mathscr{P}|_{t-\tau}^{t}$. This guarantees that the robot does not intervene between the vehicles.

By doing so, the problem is put into the framework of Section 4. Conversely to the preceding examples, now the body $D(t)$ is not rigid and may wriggle during the motion.

The speed $V$ and the maneuver of the leader or the navigation law driving it are not known to the escort robot. At the same time, it knows $\rho$ and estimates of the linear and rotational velocities of the leader:

$$0 < \underline{V} \le V \le \overline{V}, \qquad |\omega| \le \overline{\omega}. \tag{26}$$

Pursuing its own objective, the leader takes into account the escort robot by avoiding maneuvers that make the escort impossible or entail a singular situation, like e.g., those from Fig. 5(a,b). (In (a),

[5] The distance is measured along the path.

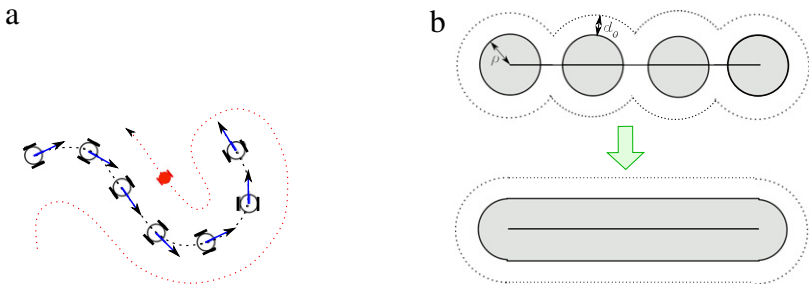


**Fig. 4.** (a) Escort mission. (b) Enhancement of the safety requirement.

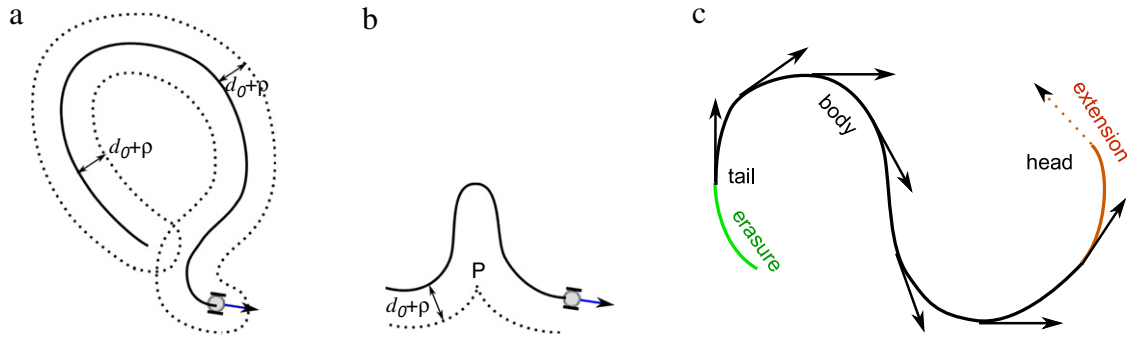


**Fig. 5.** (a,b) Singular cases for escort. (c) Motion of the boundary sides.

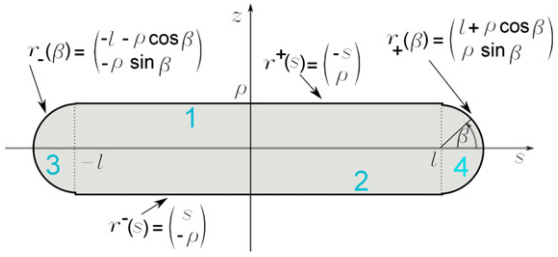


**Fig. 6.** Boundary parametrization and enumeration of its parts.

the robot can neither enter nor exit the inner dotted loop while maintaining the distance $d_0$; in (b), the robot cannot pass the cusp $P$ due to inability of instantaneous turns.) This means [45, Chapter 16] that for any path $\mathscr{P}|_{t-\tau}^{t}$ traced by the leader during $\tau$ time units, any point at the distance $\leq d_0+\rho$ from $\mathscr{P}|_{t-\tau}^{t}$ **(i)** has only one minimum distance point on $\mathscr{P}|_{t-\tau}^{t}$ and **(ii)** is not focal for this path. (These are true if $\rho+d_0$ is small enough [45, Chapter 16].) Due to (26), the tight lower bound on the path curvature radius is $\underline{V}/\overline{u}$. So **(ii)** brings the following assumption

$$\rho+d_0<\frac{\underline{V}}{\overline{\omega}}.$$

These assumptions imply that the convoy does not collide with itself and that $D(t)$ has a smooth boundary [45, Chapter 16].

Let the escort robot be driven by the navigation law (3). (We assume that the sensor system permits the robot to access the distance $d(t)$ from it to $D(t)$.) To check the assumptions from Section 4, the reference configuration of $D(t)$ is taken to be that related to the straight path. We parameterize its boundary as is shown in Fig. 6, where $l:=1/2V\tau$. The '$\pm$-side' $S^{\pm}$ of the boundary $\partial D(t)$ (i.e., the part parameterized by $\boldsymbol{r}^{\pm}(s)$) move via extension of the head and erasure of the tail, whereas their points remain on the $\rho$-equidistant curve $\mathfrak{C}^{\pm}$ of the leader path and move with the constant speed $V$ along this curve; see Fig. 5(c). So for $\boldsymbol{r}\in S^{\pm}$, the velocity does depend on time $\vec{V}(\boldsymbol{r})=\mp V\vec{T}(\boldsymbol{r})$. Let $\varkappa^{\pm}(\boldsymbol{r})$ denote the curvature of $\mathfrak{C}^{\pm}$ at the point $\boldsymbol{r}$. Then for $\boldsymbol{r}\in S^{\pm}$,

$$V_T=\mp V,\qquad V_N=0,\qquad \sigma=\langle\vec{V}_{\boldsymbol{r}}'T;\vec{N}\rangle\overset{(5)}{=}\mp V\varkappa^{\pm}(\boldsymbol{r}),$$
$$A_N\overset{(6)}{=}\langle\vec{V}_{\boldsymbol{r}}'\vec{V};\vec{N}\rangle=V^2\varkappa^{\pm}(\boldsymbol{r}),\qquad \xi\overset{(8)}{=}\pm V\overset{\star}{\pm}v,$$

where $\star$ signals that the sign in this $\pm$ is independent of the signs in the others. So dropping $\boldsymbol{r}$ in $\varkappa^{\pm}(\boldsymbol{r})$, we have by (8)

$$\mathscr{A}=V^2\varkappa^{\pm}+\frac{\mp2V\varkappa^{\pm}\xi+\varkappa^{\pm}\xi^2-d_0V^2(\varkappa^{\pm})^2}{1+\varkappa^{\pm}d_0}$$
$$=\varkappa^{\pm}\frac{V^2\mp2V\xi+\xi^2}{1+\varkappa^{\pm}d_0}=\varkappa^{\pm}\frac{(\xi\mp V)^2}{1+\varkappa^{\pm}d_0}=\frac{v^2}{(\varkappa^{\pm})^{-1}+d_0}.$$

Hence the second inequality from (10) now takes the form

$$\frac{v}{\overline{u}}\leq\lambda_a|(\varkappa^{\pm})^{-1}+d_0| \tag{27}$$

and means that the minimal turning radius of the escort robot (2) is less than the curvature radius of the $d_0$-equidistant curve of the side $S^{\pm}$, which is the expression in $[\ldots]$. Let $\boldsymbol{r}_0(t):=[X(t),Y(t)]^{\top}$ denote the position of the leader. By parameterizing $S^{\pm}$ as follows

$$\boldsymbol{r}(s)=\boldsymbol{r}_0(t_s^{\mp})\pm\rho\vec{e}_{\perp}[\alpha(t_s^{\mp})],\quad t_s^{\mp}:=t-\frac{\tau}{2}\mp\frac{s}{V},s\in[-l,l],$$

it is straightforward to compute the curvature radius $(\varkappa^{\pm}[\boldsymbol{r}(s)])^{-1}=\rho\mp\frac{V}{\omega}$. This converts (27) into

$$\frac{v}{\overline{u}}\leq\lambda_a\left|\pm\frac{V}{\omega}+\rho+d_0\right|,$$

which holds for all maneuvers obeying (26) if and only if

$$\frac{v}{\overline{u}}\leq\lambda_a\left[\frac{\underline{V}}{\overline{\omega}}-(\rho+d_0)\right]<\frac{\underline{V}}{\overline{\omega}}-(\rho+d_0). \tag{28}$$

Now we proceed to analysis of the second inequality from (10) for the front and rear half-circle parts of the body (see Fig. 6).

Putting $\vec{e}(\alpha) := [\cos\alpha, \sin\alpha]^\top$, $\vec{e}_\perp(\alpha) := [-\sin\alpha, \cos\alpha]^\top$, $t_*^+ := t$, $t_*^- := t-\tau$, we observe that

$$\underbrace{\Phi[\boldsymbol{r}_\pm(\beta), t]}_{\boldsymbol{r}_\pm(\beta,t)} = \boldsymbol{r}_0(t_*^\pm) \pm \rho\{\vec{e}[\alpha(t_*^\pm)]\cos\beta + \vec{e}_\perp[\alpha(t_*^\pm)]\sin\beta\}.$$

$$T[\boldsymbol{r}_\pm(\beta), t] = \mp\vec{e}[\alpha(t_*^\pm)]\sin\beta \pm \vec{e}_\perp[\alpha(t_*^\pm)]\cos\beta,$$
$$N[\boldsymbol{r}_\pm(\beta), t] = \mp\vec{e}[\alpha(t_*^\pm)]\cos\beta \mp \vec{e}_\perp[\alpha(t_*^\pm)]\sin\beta;$$
$$\vec{V}[\boldsymbol{r}_\pm(\beta,t), t] = [V \mp \rho\omega(t_*^\pm)\sin\beta]\vec{e}[\alpha(t_*^\pm)] \pm \rho\omega(t_*^\pm)\cos\beta\vec{e}_\perp[\alpha(t_*^\pm)];$$
$$V_T[\boldsymbol{r}_\pm(\beta), t] = \mp V\sin\beta + \rho\omega(t_*^\pm),$$
$$V_N[\boldsymbol{r}_\pm(\beta), t] = \mp V\cos\beta, \qquad \sigma[\boldsymbol{r}_\pm(\beta,t), t] = \omega(t_*^\pm),$$
$$A_N[\boldsymbol{r}_\pm(\beta,t), t] = \mp V\omega(t_*^\pm)\sin\beta + \rho\omega^2(t_*^\pm).$$

The inequality $|V_N| \le \lambda_v v$ from (10) should be true for all $\beta \in [-\pi/2, \pi/2]$. This means that the escort robot is faster than the convoyed vehicles: $V < \lambda_v v < v$. Furthermore,

$$\xi[\boldsymbol{r}_\pm(\beta,t), t] = \pm V\sin\beta - \rho\omega(t_*^\pm) \stackrel{\star}{\pm} \sqrt{v^2 - V^2\cos^2\beta},$$
$$\kappa[\boldsymbol{r}_\pm(\beta,t), t] = \rho^{-1},$$
$$\mathscr{A} = \mp V\omega(t_*^\pm)\sin\beta + \rho\omega^2(t_*^\pm) + \frac{2\omega\xi + \rho^{-1}\xi^2 - d_0\omega^2}{1+\rho^{-1}d_0} = \mp V\omega(t_*^\pm)\sin\beta + \frac{(\xi+\rho\omega)^2}{\rho+d_0}.$$

Hence the second condition from (10) takes the form

$$\frac{\left|\mp V\omega(t_*^\pm)\sin\beta + \frac{(V\sin\beta \stackrel{\star}{\pm} \sqrt{v^2-V^2\cos^2\beta})^2}{\rho+d_0}\right|}{\sqrt{v^2 - V^2\cos^2\beta}} \le \lambda_a\bar{u}.$$

Due to arbitrary choice of the signs in $\pm$'s and $\omega$ within the range (26), this is transformed into

$$\frac{V\bar{\omega}|\sin\beta| + \frac{(V|\sin\beta| + \sqrt{v^2 - V^2 + V^2\sin^2\beta})^2}{\rho+d_0}}{\sqrt{v^2 - V^2 + V^2\sin^2\beta}} \le \lambda_a\bar{u}.$$

Via checking the derivative sign, it is easy to see that the left-hand side is an increasing function of $V|\sin\beta|$, which ranges over $[0, \bar{V}]$ as $\beta$ and $V$ run over $[-\pi/2, \pi/2]$ and $[\underline{V}, \bar{V}]$, respectively. So the inequality holds for all these $\beta$ and $V$ if and only if it is true for $\beta := \pi/2$ and $V := \bar{V}$:

$$\bar{V}\bar{\omega} + \frac{(\bar{V}+v)^2}{\rho+d_0} \le \lambda_a\bar{u}v < \bar{u}v. \tag{29}$$

Summarizing, we see that Assumptions 1–5 hold for all feasible scenarios if and only if $\bar{V} < v$ and (28), (29) are true. Moreover, these requirements are 'almost necessary' for the robot to be capable of escorting the convoy irrespective of the scenario within the range (26). By Lemma 5.1, they are simultaneously sufficient for the navigation law (3) to ensure locally stable escort at the distance $d_0$ if $\delta$, $\gamma$ in Fig. 1(b) are chosen so that (14) holds. In (14), $\eta_\nu \in (0, 1-\lambda_\nu)$, $\nu = v, a$ and according to the last paragraph from Section 5, $z_* > 0$ is chosen so that the following system of linear and quadratic (in $z_*$) inequalities is satisfied

$$z_* \le \eta_a\bar{u}\left[\frac{\underline{V}}{\bar{\omega}} - (\rho+d_0)\right], \qquad z_* < \frac{v}{\sqrt{2}-1},$$
$$\frac{2(\bar{V}+v)z_* + z_*^2}{\rho+d_0} + (\lambda_a+\eta_a)\frac{z_*}{\sqrt{2}-1} < \eta_a\bar{u}v.$$

(This system is consistent and holds for all small enough $z_*$.)

Analysis similar to that from the previous subsection shows that for non-local convergence (i.e., for the conclusion of Theorem 1 to be valid) it suffices that Assumption 7 is true and (29), (29) are valid with $d_0 := \max\{d_0, d_+\}$ and $d_0 := \min\{d_0, d_-\}$, respectively. Here $d_-$ and $d_+$ are the minimal and maximal distances, respectively, from the points of the union of the initial circles to $D(t)$ within the first $\frac{3\pi}{\bar{u}}$ time units of motion. In the controller design, the parameter $z_*$ should be taken as the minimum among the values calculated in accordance with the above recommendations for $d_0 := \max\{d_0, d_+\}$ and $d_0 := \min\{d_0, d_-\}$, respectively.

**Table 1**
Some geometrical, kinematic, and dynamical parameters.

| No. | $T$ | $N$ | $\sigma$ | $V_T$ |
|---|---|---|---|---|
| 1, 2 | $\mp\begin{pmatrix}1\\0\end{pmatrix}$ | $\mp\begin{pmatrix}0\\1\end{pmatrix}$ | $\omega$ | $\mp V + \rho\omega$ |
| 3, 4 | $\pm\begin{pmatrix}-\sin\beta\\\cos\beta\end{pmatrix}$ | $\mp\begin{pmatrix}\cos\beta\\\sin\beta\end{pmatrix}$ | $\omega$ | $\omega\rho + \omega l\cos\beta \mp V\sin\beta$ |

| No. | $V_N$ | $A_N$ | $\kappa$ |
|---|---|---|---|
| 1, 2 | $\omega x'$ | $\mp\omega V + \dot{\omega}x' + \omega^2\rho$ | 0 |
| 3, 4 | $\mp V\cos\beta - \omega l\sin\beta$ | $\omega^2\rho - \dot{\omega}l\sin\beta \mp \omega V\sin\beta + \omega^2 l\cos\beta$ | $\frac{1}{\rho}$ |

### 6.5. Escorting a Bulky Cigar-shaped vehicle

The body $D(t)$ is a rigid and cigar-shaped vehicle, as is shown in Fig. 3(b). It moves forward with the constant speed $V$ in the direction of its centerline, which is time-varying. The motion is described by the unicycle-like Eqs. (25), where $X$ and $Y$ are the abscissa and ordinate, respectively, of the vehicle center in the world frame and $\alpha$ gives the centerline orientation. The speed $V$ and the maneuver of the body or the navigation law driving it are not known. At the same time, the shape parameters $l$ and $\rho$ from Fig. 3(b) are known, and the speed, as well as the rotational velocity and acceleration of $D$ can be upper bounded by known constants:

$$0 \le V \le \bar{V}, \qquad |\omega| \le \bar{\omega}, \qquad |\dot{\omega}| \le \aleph. \tag{30}$$

In the reference frame attached to the body, $\partial D$ can be parameterized as is shown in Fig. 6. In this frame,

$$\vec{V} = V\begin{pmatrix}1\\0\end{pmatrix} + \omega\mathscr{R}_{\frac{\pi}{2}}\boldsymbol{r}, \qquad \vec{A} = \omega V\begin{pmatrix}0\\1\end{pmatrix} + \dot{\omega}\mathscr{R}_{\frac{\pi}{2}}\boldsymbol{r} - \omega^2\boldsymbol{r}.$$

Elementary computation results in Table 1, where No. refers to the serial number of the boundary part introduced in Fig. 6, and in $\pm$ and $\mp$, the upper and lower signs correspond to the parts with odd and even numbers, respectively. By substituting data from this table into (10), we see that the first inequality from (10) takes the form

$$\max_{|s|\le l}|\omega s| \le \lambda_v v, \qquad \max_{|\beta|\le\pi/2}|\mp V\cos\beta - \omega l\sin\beta| \le \lambda_v v$$

and after calculating these maxima, shapes into $\sqrt{V^2 + \omega^2 l^2} \le \lambda_v v$. This inequality is satisfied for all scenarios within the range (30) if and only if

$$V_\omega := \sqrt{\bar{V}^2 + \bar{\omega}^2 l^2} \le \lambda_v v < v. \tag{31}$$

Similarly the second inequality from (10) written for the straight parts of the boundary shapes into

$$\frac{|\pm V\omega - \omega^2(\rho+d_0) + \dot{\omega}s \stackrel{\star}{\pm} 2\omega\sqrt{v^2 - \omega^2 s^2}|}{\sqrt{v^2 - \omega^2 s^2}} \le \lambda_a\bar{u}.$$

It is clear that this inequality holds for all $V$ and $\dot{\omega}$ within the range (30) if and only if

$$\frac{\bar{V}|\omega| + \omega^2(\rho+d_0) + \aleph|s|}{\sqrt{v^2 - \omega^2 s^2}} + 2|\omega| \le \lambda_a\bar{u}.$$

Here the left-hand side increases as $|\omega|$ or $|s|$ grows. So the second inequality from (10) holds for the straight parts of the boundary and all feasible scenarios if and only if

$$\frac{\overline{V}\overline{\omega}+\overline{\omega}^2(\rho+d_0)+\aleph l}{\sqrt{v^2-\overline{\omega}^2 l^2}}+2\overline{\omega}\le\lambda_a\overline{u}<\overline{u}. \tag{32}$$

For the circular parts, we have due to (8),

$$\begin{aligned}\mathscr{A}&=A_N+\frac{2\omega\xi+\rho^{-1}\xi^2-d_0\omega^2}{1+\rho^{-1}d_0}=\omega^2\rho-\dot{\omega}l\sin\beta\\&\quad+\omega\underbrace{[\mp V\sin\beta+\omega l\cos\beta]}_{=:V_\beta}+\frac{2\omega\rho\xi+\xi^2-\rho d_0\omega^2}{\rho+d_0}\\&=\omega V_\beta-\dot{\omega}l\sin\beta+\frac{(\xi+\rho\omega)^2}{\rho+d_0}.\end{aligned}$$

By Table 1, $V_N=\mp V\cos\beta-\omega l\sin\beta$ and so $V_N^2+V_\beta^2=V^2+\omega^2l^2$, $\sqrt{v^2-V_N^2}=\sqrt{\Delta^2+V_\beta^2}$, where $\Delta:=\sqrt{v^2-V^2-\omega^2l^2}$ is well defined by (31). Hence with regard to (8), $\xi+\omega\rho=-\omega\rho-\omega l\cos\beta\pm V\sin\beta\pm\sqrt{\Delta^2+V_\beta^2}+\omega\rho=-V_\beta\pm\sqrt{\Delta^2+V_\beta^2}$. Overall, the examined second inequality from (10) now looks as follows:

$$\frac{\left|\omega V_\beta-\dot{\omega}l\sin\beta+\frac{(V_\beta\mp\sqrt{\Delta^2+V_\beta^2})^2}{\rho+d_0}\right|}{\sqrt{\Delta^2+V_\beta^2}}\le\lambda_a\overline{u}.$$

This holds for all scenarios satisfying (30) if and only if

$$\max_{\substack{|\omega|\le\overline{\omega}\\0\le V\le\overline{V}\\|\beta|\le\frac{\pi}{2}}}\left[\frac{\aleph l|\sin\beta|}{\sqrt{\Delta^2+V_\beta^2}}+\frac{\left|\omega V_\beta+\frac{(V_\beta\mp\sqrt{\Delta^2+V_\beta^2})^2}{\rho+d_0}\right|}{\sqrt{\Delta^2+V_\beta^2}}\right]\le\lambda_a\overline{u}.$$

It can be shown that the first and second addends differently behave as $\beta$ runs over its range $[-\pi/2,\pi/2]$, which troubles explicit computation of the maximum. To proceed analytically, we inject some non-conservatism by upper estimating the maximum of the sum by the sum of the maxima of the addends, thus substituting the following stronger condition in place of the above one

$$\max_{\substack{|\omega|\le\overline{\omega}\\0\le V\le\overline{V}\\|\beta|\le\frac{\pi}{2}}}\underbrace{\frac{\aleph l|\sin\beta|}{\sqrt{\Delta^2+V_\beta^2}}}_{\Upsilon}+\max_{\substack{|\omega|\le\overline{\omega}\\0\le V\le\overline{V}\\|\beta|\le\frac{\pi}{2}}}\underbrace{\frac{\left|\omega V_\beta+\frac{(V_\beta\mp\sqrt{\Delta^2+V_\beta^2})^2}{\rho+d_0}\right|}{\sqrt{\Delta^2+V_\beta^2}}}_{\Xi}\le\lambda_a\overline{u}. \tag{33}$$

Given $\beta$, a larger value $\Upsilon$ is provided by the sign in $\mp$ that makes the signs of the addends in $V_\beta=\mp V\sin\beta+\omega l\cos\beta$ opposite. Hence the first maximum equals

$$\max_{\substack{|\omega|\le\overline{\omega}\\0\le V\le\overline{V}\\0\le\beta\le\frac{\pi}{2}}}\underbrace{\frac{\aleph l\sin\beta}{\sqrt{\Delta^2+(|\omega|l\cos\beta-V\sin\beta)^2}}}_{\Psi}.$$

It is easy to check that $\Psi'_\beta\ge0\ \forall\beta\in[0,\pi/2]$. So the maximum over $\beta$ is attained at $\beta=\pi/2$, and the entire maximum equals $\frac{\aleph l}{\sqrt{v^2-\overline{\omega}^2l^2}}$.

As for $\Xi$, we note that the expression $V_\beta$ with $+$ in $\pm$ equals $V_{-\beta}$ with $-$, whereas the range $[-\pi/2,\pi/2]$ of $\beta$ is symmetric. This permits us to neglect one of the sign options by considering only $V_\beta=\omega l\cos\beta+V\sin\beta$. Then $\Xi=\Xi(V_\beta,V,\omega)$, where $V_\beta$ ranges over $[-V,\sqrt{V^2+\omega^2l^2}]$ for $\omega\ge0$ and over $[-\sqrt{V^2+\omega^2l^2},V]$ for $\omega<0$. For $V_\beta\in[-V,V]$, the maximum of $\Xi$ over all possible combinations of the signs in $\Xi$ and $\pm\omega$, $\pm V_\beta$ evidently equals

$$\frac{|\omega||V_\beta|+\frac{(|V_\beta|+\sqrt{\Delta^2+V_\beta^2})^2}{\rho+d_0}}{\sqrt{\Delta^2+V_\beta^2}}.$$

For the remaining parts ($V_\beta\in[V,\sqrt{V^2+\omega^2l^2}]$ for $\omega\ge0$ and $V_\beta\in[-\sqrt{V^2+\omega^2l^2},-V]$ for $\omega<0$) the same is true with respect to the maximum over two signs in $\Xi$. Thus we see that the second maximum in (33) is equal to

$$\begin{aligned}&\max_{\substack{0\le\omega\le\overline{\omega}\\0\le V\le\overline{V}\\0\le V_\beta\le\sqrt{V^2+\omega^2l^2}}}\frac{\omega V_\beta+\frac{(V_\beta+\sqrt{\Delta^2+V_\beta^2})^2}{\rho+d_0}}{\sqrt{\Delta^2+V_\beta^2}}\\&=\max_{\substack{0\le\omega\le\overline{\omega}\\0\le V\le\overline{V}\\0\le V_\beta\le\sqrt{V^2+\omega^2l^2}}}\left[\omega\frac{V_\beta}{\sqrt{\Delta^2+V_\beta^2}}+\frac{1}{\rho+d_0}\left(\frac{V_\beta^2}{\sqrt{\Delta^2+V_\beta^2}}+2V_\beta+\sqrt{\Delta^2+V_\beta^2}\right)\right].\end{aligned}$$

It is easy to check that in the last expression, all addends increase as $V_\beta$ grows. Thus the maximum over $V_\beta$ is attained at $V_\beta=\sqrt{V^2+\omega^2l^2}$ and the entire maximum is equal to

$$\max_{\substack{0\le\omega\le\overline{\omega}\\0\le V\le\overline{V}}}\frac{\omega\sqrt{V^2+\omega^2l^2}+\frac{(\sqrt{V^2+\omega^2l^2}+v)^2}{\rho+d_0}}{v}.$$

Overall, the second condition from (10) for the circular parts is implied by the inequality (where $V_\omega$ is taken from (31)):

$$\frac{\aleph l}{\sqrt{v^2-\overline{\omega}^2l^2}}+\frac{\overline{\omega}V_\omega+\frac{(V_\omega+v)^2}{\rho+d_0}}{v}\le\lambda_a\overline{u}<\overline{u}. \tag{34}$$

Bringing the pieces together, we see that Assumptions 1–5 hold for all feasible scenarios if (31), (32) and (34) are true. Moreover, these requirements are sufficient for the navigation law (3) to ensure locally stable patrolling if $\delta$, $\gamma$ in Fig. 1(b) are chosen so that (14) holds, where $\eta_\nu\in(0,1-\lambda_\nu)$, $\nu=v,a$ and according to the last paragraph from Section 5, $z_*\in(0,\frac{v}{\sqrt{2}-1})$ is chosen so that (32) and (34) are true with $\lambda_a:=\lambda_a+\eta_a$ and under substitution in place of $v$ an arbitrary value from the interval $[v-\frac{z_*}{\sqrt{2}-1},v+z_*]$. This evidently holds if $z_*$ is chosen small enough so that

$$\frac{\overline{V}\overline{\omega}+\overline{\omega}^2(\rho+d_0)+\aleph l}{\sqrt{\left(v-\frac{z_*}{\sqrt{2}-1}\right)^2-\overline{\omega}^2l^2}}+2\overline{\omega}\le(\lambda_a+\eta_a)\overline{u},$$

$$\frac{\aleph l}{\sqrt{\left(v-\frac{z_*}{\sqrt{2}-1}\right)^2-\overline{\omega}^2l^2}}+\frac{\overline{\omega}V_\omega+\frac{(V_\omega+v+z_*)^2}{\rho+d_0}}{v-\frac{z_*}{\sqrt{2}-1}}\le(\lambda_a+\eta_a)\overline{u}.$$

Analysis similar to that from the previous subsections also shows that for non-local convergence (i.e., for the conclusion of Theorem 1 to be valid) it suffices that Assumption 7 is true, (32) is true with $d_0:=\max\{d_0,d_+\}$ and (34) is valid with $d_0:=\min\{d_0,d_-\}$. The parameter $z_*$ should be taken as the minimum among the values calculated in accordance with the above recommendations for $d_0:=\min\{d_-,d_0\}$ and $d_0:=\max\{d_+,d_0\}$, respectively.

## 7. Guidance in an environment cluttered with moving obstacles

Now we consider a more general problem of vehicle guidance with obstacle avoidance. There is a steady point target $\boldsymbol{T}$ and several constantly disjoint moving obstacles $D_1(t), \ldots, D_k(t)$ in the plane. The objective is to drive the vehicle to the target through the obstacle-free part of the plane: $\boldsymbol{r}(t) \notin \bigcup_{i=1}^{k} D_i(t)\ \forall t$. Moreover, a given safety margin must be respected: $\mathbf{dist}_{D_i(t)}[\boldsymbol{r}(t)] \geq d_{\text{safe}} \geq 0\ \forall t, i$.

Our proposed controller switches between the obstacle avoidance law (3) and straight moves to $\boldsymbol{T}$:

$$u(t) = 0. \tag{35}$$

In (3), $d_0 > d_{\text{safe}}$ is now a tunable controller parameter (the desired distance to the obstacle during bypassing it) and $d(t)$ is replaced by $d_i(t) := \mathbf{dist}_{D_i(t)}[\boldsymbol{r}(t)]$ for $i$ chosen by the controller. There are two more controller parameters:

- $\epsilon > 0$ — participates to decision of obstacle avoidance termination, which is allowed only if the robot comes close enough to the obstacle: $d_i \leq d_0 + \epsilon$;
- $C > d_0 + \epsilon$ — the trigger threshold: the distance to an obstacle at which the avoidance mode is switched on.

The switch (35) $\mapsto$ (3) occurs when the distance $d_i$ to the obstacle $D_i(t)$ reduces to $C$, with this $i$ being employed $d := d_i$ in (3). The converse (3) $\mapsto$ (35) is carried out when $d_i(t) \leq d_0 + \epsilon$ and the vehicle is headed towards the target. For this rule to be well-defined, (3) must not be activated simultaneously for several obstacles. To offer constructive conditions for this to hold, we introduce the following.

**Definition 4.** The *averaged span* of obstacle $i$ is $\mathscr{R}_i^{\text{av}} = \min \mathscr{R}_i$, where min is over all $\mathscr{R}_i$ such that during any time interval of duration $(3\pi)/\overline{u}$ the body $D_i(t)$ remains in some steady disc of the radius $\mathscr{R}_i$.

By **iii** of Theorem 1, since the start of the avoidance maneuver at the distance $C$ from obstacle $i$ and until the commencement of the sliding motion towards the $d_0$-equidistant curve, the robot moves inside the disc of the radius $2R$ centered at its initial position, where $R$ is given by (2). Meanwhile the obstacle moves within some disc of the radius $\mathscr{R}_i^{\text{av}}$. So at this phase, the distance $d_i$ from the robot to the obstacle constantly lies in the interval

$$d_i \in [C - 2(R + \mathscr{R}_i^{\text{av}}); C + 2(R + \mathscr{R}_i^{\text{av}})]. \tag{36}$$

Afterward $d_i$ monotonically goes to $d_0 < C$ by Theorem 1. Thus while the navigation rule (3) is active for obstacle $i$, the robot is at the distance $\leq C + 2(R + \mathscr{R}_i^{\text{av}})$ from $D_i(t)$. So to exclude simultaneous activation of this rule for two obstacles, it suffices that they are separated by the distance $> 2(C + R + \mathscr{R}_{\max}^{\text{av}})$, where $\mathscr{R}_{\max}^{\text{av}} := \max_i \mathscr{R}_i^{\text{av}}$. With regard to the available freedom in the choice of $C, d_0, \epsilon$ ($C > d_0 + \epsilon, \epsilon > 0, d_0 > d_{\text{safe}}$), this gives rise to the following requirement to the distance $d_{i,j}(t)$ between any two obstacles $i, j$:

$$d_{i,j}(t) \geq d_{\text{obs}} > 2(R + \mathscr{R}_{\max}^{\text{av}} + d_{\text{safe}}) \quad \forall i \neq j. \tag{37}$$

Then $C, d_0$ and $\epsilon$ may and should be chosen so that

$$\frac{d_{\text{obs}}}{2} - (R + \mathscr{R}_{\max}^{\text{av}}) > C > d_0 + \epsilon, \quad \epsilon > 0,\ d_0 > d_{\text{safe}}.$$

Since the navigation law (3) is still employed, the conditions for its convergence should be satisfied. We suppose that Assumptions 1 and 2 hold for any obstacle. If $C \geq 2(R + \mathscr{R}_{\max}^{\text{av}})$, the aforementioned two discs do not intersect (see Fig. 7(a)) and so can be separated by a straight line; thus Assumption 7 holds. Such a choice

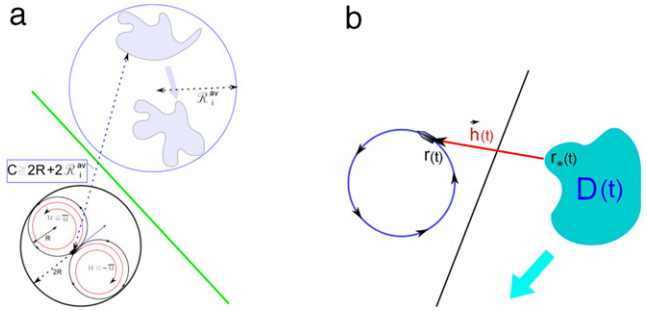


**Fig. 7.** (a) Non-intersecting discs. (b) Vector $\vec{h}(t)$.

of $C$ is possible only if $d_{\text{obs}} > 6R + 6\mathscr{R}_{\max}^{\text{av}}$ in addition to (37), which is assumed. Accordingly, $C$ should be chosen so that

$$\frac{d_{\text{obs}}}{2} - (R + \mathscr{R}_{\max}^{\text{av}}) > C > \max\{d_0 + \epsilon; 2(R + \mathscr{R}_{\max}^{\text{av}})\}. \tag{38}$$

As for Assumption 6, we note that due to (36), all launching distances for any maneuver of bypassing obstacle $i$ are contained by the interval from (36) and so by

$$[C - 2(R + \mathscr{R}_{\max}^{\text{av}}); C + 2(R + \mathscr{R}_{\max}^{\text{av}})]. \tag{39}$$

So Assumption 6 can be satisfied if within the range (38), there is a value of $C$ such that $C - 2(R + \mathscr{R}_{\max}^{\text{av}}) > d_{\text{safe}}$, and the interval (39) is regular for any obstacle, provided that $d_0$ is chosen within this interval. Overall, we arrive at the following recommendations on the choice of $C, d_0, \epsilon$

$$\begin{aligned}
&2(R + \mathscr{R}_{\max}^{\text{av}}) > \epsilon > 0,\\
&\frac{d_{\text{obs}}}{2} - (R + \mathscr{R}_{\max}^{\text{av}}) > d_0 > d_{\text{safe}},\\
&\min\left\{\frac{d_{\text{obs}}}{2} - (R + \mathscr{R}_{\max}^{\text{av}}); d_0 + 2(R + \mathscr{R}_{\max}^{\text{av}})\right\}\\
&\quad > C\\
&\quad > \max\{d_0 + \epsilon; 2(R + \mathscr{R}_{\max}^{\text{av}}) + d_{\text{safe}}\}.
\end{aligned} \tag{40}$$

This is possible if and only if $d_{\text{obs}} > 6R + 6\mathscr{R}_{\max}^{\text{av}} + 2d_{\text{safe}}$.

To properly choose the controller parameters $\gamma$ and $\delta$, it suffices to pick the auxiliary parameters $z_*, \lambda_a, \lambda_v, \eta_a, \eta_v$ in (37) common for all obstacles. This is possible: for every obstacle, $\lambda_a, \lambda_v$ in (10) are first increased (within $(0, 1)$) to a common value, then common $\eta_v \in (0, 1-\lambda_v)$, $\eta_a \in (0, 1-\lambda_a)$ are picked. Finally, $z_*$ is computed for all obstacles and the minimal result is put in (37).

For the proposed guidance law (PGL) to be implementable, the robot should have access to the angle-of-sight $\beta(t)$ to the target $T$, as well as to the distance $d_i$ and its derivative $\dot{d}_i$ whenever $d_i \leq C + 2R + 2\mathscr{R}_i^{\text{av}}$. We also assume that initially the vehicle is above the trigger threshold of all obstacles $d_i(0) > C\ \forall i$ and that they are always far enough from the target $\mathbf{dist}_{D_i(t)}[\boldsymbol{T}] > d_0 + \epsilon\ \forall t, i$. Since the controller (3) is still used, conditions (10) and (14) should be also replicated.

In this paper, the convergence and performance of PGL for target reaching with obstacle avoidance is demonstrated via extensive simulations and experimental studies. They are presented in the next two sections.

## 8. Simulations

Matlab and MobileSim0.5 (a simulator for ActivMedia robots) were used to illustrate the performance of the proposed guidance law (PGL); the simulation parameters are given in Table 2, where $T_s$ is the sampling period. The derivative $\dot{d}$ was approximated by the Newton's difference quotient $\dot{d}(t) \approx T_s^{-1}[d(t) - d(t - T_s)]$. The robot was navigated through environment with four moving

**Table 2**
Robot and controller sumulation parameters.

| | | | |
|---|---|---|---|
| $T_s = 0.1$ s | $\overline{u} = 0.8$ rad/s | $d_0 = 1.2$ m | $\varepsilon = 0.1$ m |
| $v = 1$ m/s | $\gamma = 1.51$/s | $d_{\text{safe}} = 1$ m | $C = 1.5$ m |

nearly rectangular shaped rigid obstacles. It has access only to the current distance to the obstacles $d(t)$. Fig. 8(a) shows the initial states of the robot and obstacles and the position of the target, Fig. 8(c), (e) and (g) display the crucial moments of the maneuver when the distance from the robot to a particular obstacle achieves its minimum. The paths of the robot and obstacles are depicted in green and blue, respectively. Fig. 8(d), (f) and (h) show the evolution of the distance from the robot to each of the obstacles. The red rectangles on Fig. 8(c), (e) and (g) illustrate the states the robot and the nearest obstacle at the above crucial moments; the minimal distance is similarly marked in Fig. 8(d), (f) and (h). In this experiment, the robot successfully arrives at the target with avoiding collisions with the moving obstacles.

The performance of PGL was compared with that of the Velocity Obstacle approach (VOA) [7,4] via simulation in MatLab in the scenario where a long obstacle perpendicularly intervenes between the robot and the target, which is hidden just behind the obstacle; see Fig. 9(a, b). Fig. 9(c, d) display the situations at the moments when the robot transverses the path of the obstacle. The entire paths of the robot during target reaching with obstacle avoidance are depicted in Fig. 9(d, f). (We considered VOA with two choices of velocity per maneuver, with the second choice being made at the favorable moment of bypassing the obstacle.) PGL first drives the robot directly to the target in a straight line until the trigger threshold is trespassed and then undertakes a relatively small de-tour by following the obstacle boundary. VOA basically drives the robot to the target along two straight lines with bypass of the obstacle in a close range at the rear. Thus the both guidance laws do drive the robot to the target. However PGL does this faster: the ratio of the maneuver times is as follows $\frac{T_{\text{PGL}}}{T_{\text{VOA}}} = \frac{14.51}{18.61} \approx 0.78$. Thus in this experiment, PGL outperforms VOA.

In the next simulation, the robot moves to the target (the red circle in Fig. 10) with bypassing a large cross rotating about a moving pivot. The translational and rotational directions of the obstacle, its initial state and that of the robot are shown in Fig. 10(a). The robot first moves towards the target until its distance to the obstacle reduces to the trigger threshold, as is shown in Fig. 10(b). Then it turns left to avoid the obstacle, as shown in Fig. 10(c). Finally, it bypasses the cross and arrives at the target, as is shown in Fig. 10(d).

Fig. 11 displays the results of simulations concerned with the problem of escorting a convoy of unicycle-like vehicles, which was described in Section 6.4. In this experiment, the leader moves with the constant speed $V = 0.3$ m/s and time-varying turning rate not exceeding $\overline{\omega} = 0.55$ rad/s, the convoy is composed of four vehicles, each approximated by a disc with the radius $\rho = 0.1$ m, moving at the distance $\Delta s = 0.133$ m one after another so that the total length of the convoy equals 1.2 m, and the desired escort distance was taken to be $d_0 = 1.5$ m. The escorting robot starts motion at a remote location. As is shown in Fig. 11(b), after a transient, the robot escorts the convoy with maintaining the desired distance 1.5 m from it with the error not exceeding 0.247 m.

## 9. Experimental results

The performance and applicability of PGL was examined on an ActivMedia Pioneer 3-DX robot. This a differential drive vehicle equipped with an onboard computing module, which can be connected to a laptop via WIFI. Other equipment includes a Sick

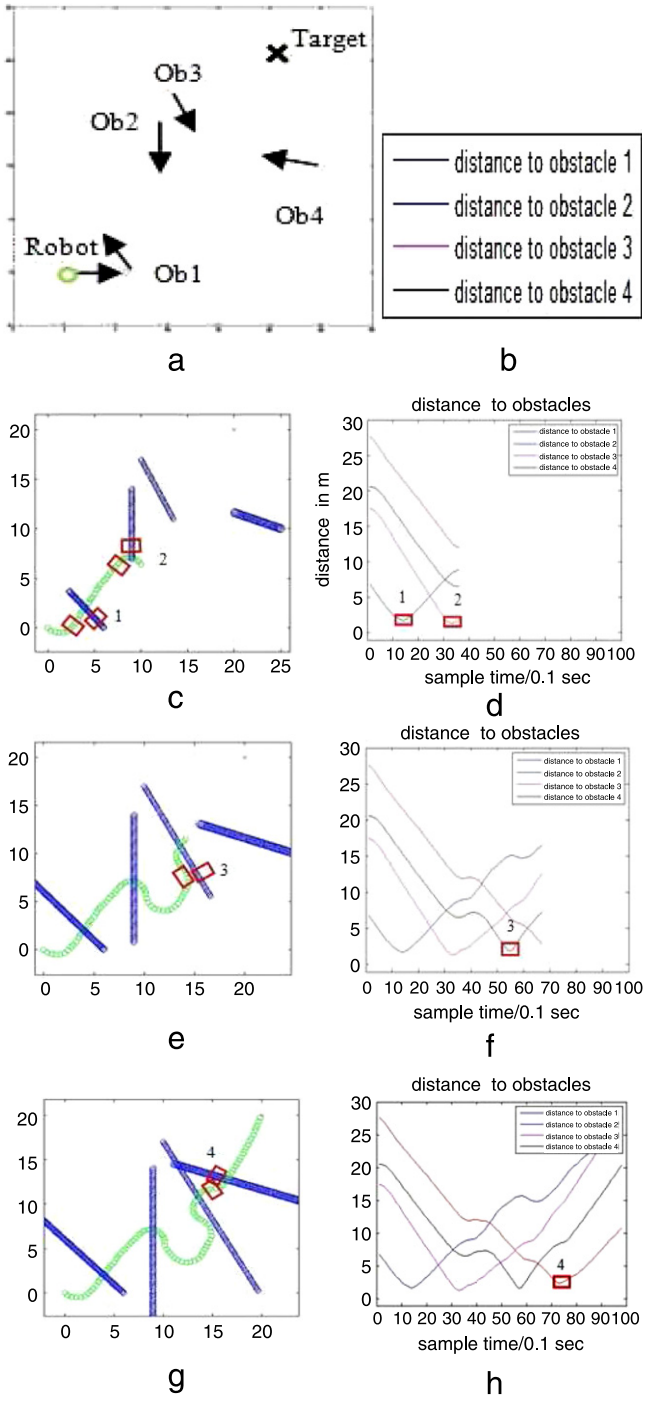


**Fig. 8.** Robot navigation in a dynamic environment.

laser range finder and 16 sonar sensors, which provide the distance and angle information about the obstacles within the predefined scan range. The robot also has access to the target angle-of-sight, the relative position of the robot is obtained via odometry. C++ programming underlaid the use of ARIA, the ActivMedia Advanced Robot Interface for Applications, which is an object oriented Linux platform C++ library providing a dynamic control of the robot's velocity, heading, relative heading, etc.

Fig. 12(a) shows an environment with five static obstacles (four boxes and one human) and black target. In Fig. 12, the trajectory of the robot at various stages of progression is depicted by the dashed lines; the dashed red circles display the trigger curves where the

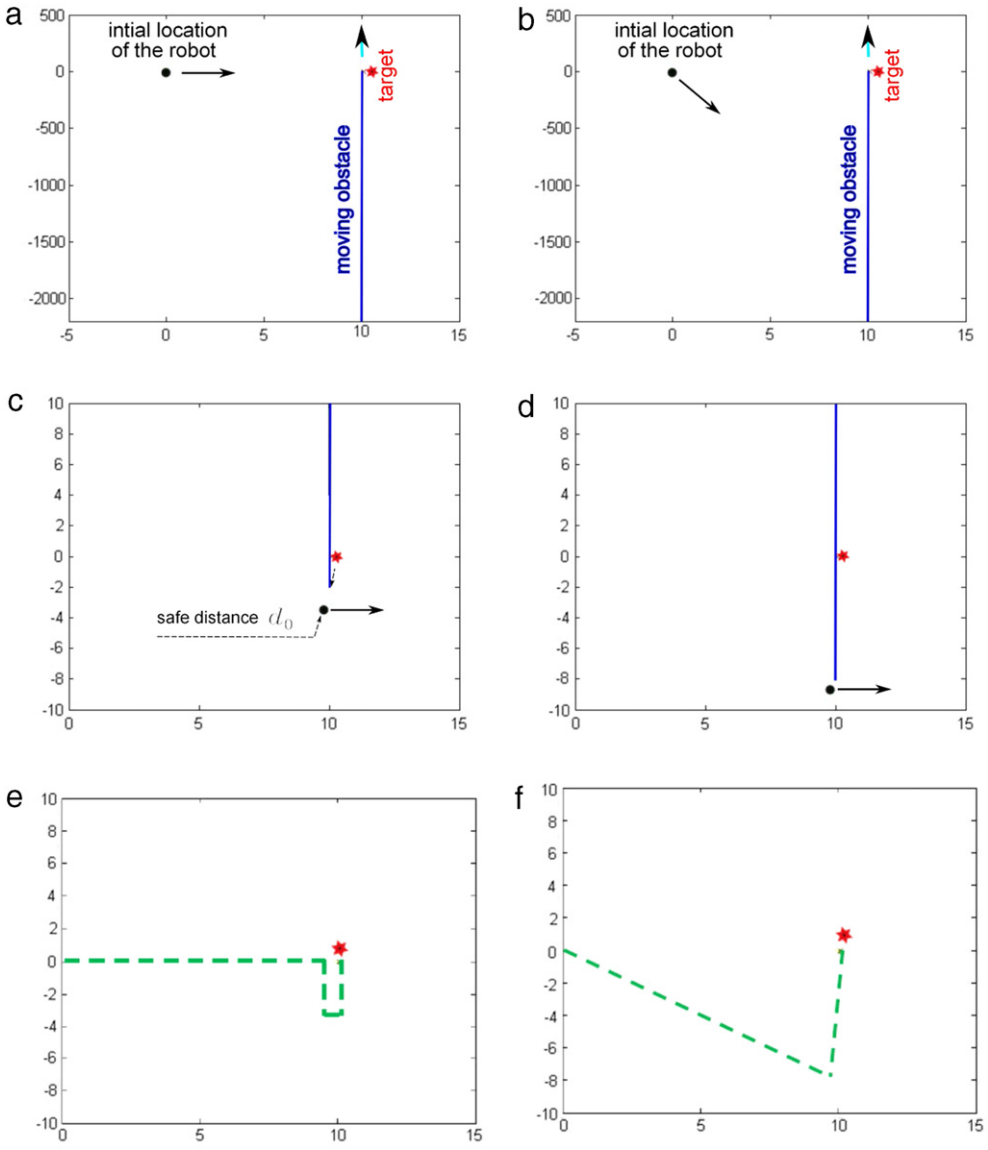


**Fig. 9.** PGL (left column) versus VOA (right column).

robot is switched to the avoidance mode. In this experiment, like in the others, the robot reaches the target via safe navigation among the obstacles, with no visible chattering of the mechanical parts being observed.

Fig. 13 concerns another experiment, where both static (the boxes) and moving (the humans) obstacles are involved. The target is positioned at the black cross. The overall path of the robot is shown in Fig. 13(e), the crucial moments during progression along the path are displayed in Fig. 13(b)–(d). The robot copes with moving obstacles as well.

In the last experiment, the influence of the parameters on the overall performance was studied. To this end, both the speed of the robot and the trigger threshold were decreased. As is shown in Fig. 14(b), this may result in bypassing an obstacle with a smaller turning maneuver, which carries a potential to decrease the deviation from the optimal motion in the straight line. However Fig. 14(c) displays the opposite: due to the reduced speed, the robot accompanies the moving obstacle for a longer time, which engages the robot in a long side maneuver. The reduced speed also caused an increase of the overall time of target reaching.

## 10. Conclusions

A sliding mode based method for a unicycle-like vehicle navigation and guidance has been presented. The proposed navigation and guidance law was applied to the problems of border patrolling and obstacle avoidance. Mathematically rigorous analysis of this law in the border patrolling scenario has been presented. The efficiency of the proposed algorithm in obstacle avoidance problems has been illustrated by computer simulations and experiments with real robots. The applicability of the proposed sliding mode controller was confirmed by the fact that no visible chattering of the mechanical parts was observed in the experiments.

## Appendix. Proofs of theoretical results

In the appendix, the Frenet frame $[\vec{T}(\boldsymbol{r}, t), \vec{N}(\boldsymbol{r}, t)]$ and the variables attributed to the motion of the domain, like $\vec{V}(\boldsymbol{r}, t), \vec{A}(\boldsymbol{r}, t)$, etc., are considered only for $\boldsymbol{r} := \boldsymbol{r}_*(t)$. With a slight abuse of notations, the resultant argument $[\boldsymbol{r}_*(t), t]$ is

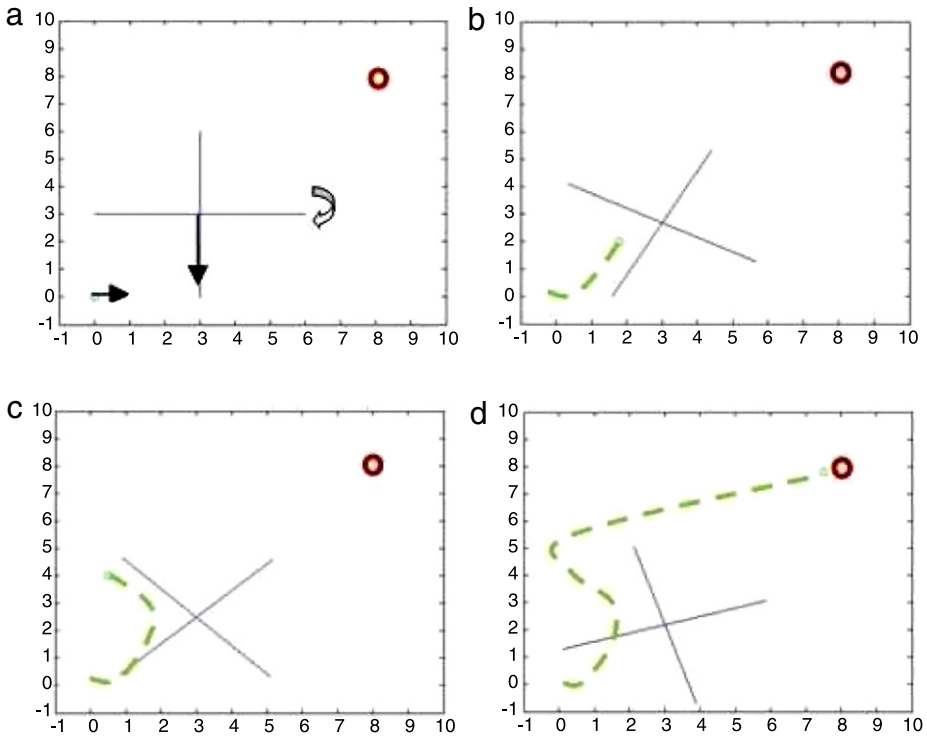


**Fig. 10.** Robot avoids a rotating obstacle.

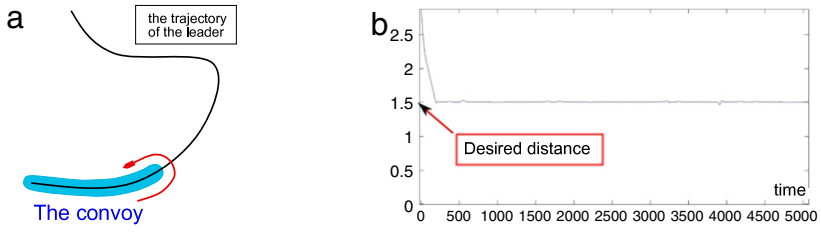


**Fig. 11.** (a) Escorting a convoy. (b) The distance to the border.

replaced by $t$ and dropped if $t$ is clear from the context. We denote by $\mathbf{Nr}[\vec{W}] := \vec{W}/\|\vec{W}\|$, $\mathbf{Pr}_{\vec{W}}$, and $\vec{W}^{\perp}$ the normalization of the vector $\vec{W}$, the orthogonal projection on the line spanned by $\vec{W}$, and the line perpendicular to $\vec{W}$, respectively; $\mathscr{R}_\theta$ is the matrix of rotation through angle $\theta$.

**Lemma A.1.** *The velocity $\vec{v}$ of the robot has the form*

$$\vec{v} = \underbrace{[\dot{s} + d\mu]}_{\xi}\vec{T} + \vec{V} - \dot{d}\vec{N}, \tag{A.1}$$

*where $\dot{s}$ is the speed of the relative motion of $\mathbf{r}_*$ along the boundary $\partial D$, i,e, $\dot{\mathbf{r}}_* - \vec{V} = \dot{s}\vec{T}$, and*

$$\mu := \langle \vec{V}'_{\mathbf{r}}\vec{T}, \vec{N}\rangle + \kappa\dot{s} = \langle \mathscr{E}\vec{T}, \vec{N}\rangle + \omega + \kappa\dot{s}. \tag{A.2}$$

*The Frenet frame evolves so that*

$$\frac{d\vec{T}}{dt} = \mu\vec{N}, \qquad \frac{d\vec{N}}{dt} = -\mu\vec{T}. \tag{A.3}$$

**Proof.** To prove (A.1) and (A.3) at a particular time instant $\tau$, we reset the reference configuration to be $D(\tau)$. This does not alter the velocity and acceleration fields and their descendants but converts $\Phi(\boldsymbol{r}, t)$ into $\Phi(\boldsymbol{r}, t|\tau) := \Phi[\Phi^{-1}(\boldsymbol{r}, \tau), t]$. Let $\boldsymbol{\rho}(s)$ stand for a regular parametric representation of $\partial D(\tau)$, where $s$ is the arc length, or natural parameter (which ascends so that $D(\tau)$ is to the left). Then

$$\boldsymbol{r}(t) = \Phi\{\boldsymbol{\rho}[s(t)], t|\tau\} - d\vec{N} \tag{A.4}$$

and $\mathbf{r}_*(t) = \Phi\{\boldsymbol{\rho}[s(t)], t|\tau\}$, whence $\dot{\boldsymbol{r}}_*(\tau) = \dot{s}(\tau)\vec{T}(\tau) + \vec{V}(\tau) \Rightarrow \dot{s} = \dot{s}(\tau)$. Since the map $s \mapsto \Phi\{\boldsymbol{\rho}[s], t|\tau\}$ provides parametric representation of $\partial D(t)$, we have

$$\vec{T}\{\Phi[\boldsymbol{\rho}(s), t|\tau]\} = \mathbf{Nr}\{\Phi'_{\boldsymbol{r}}\{\boldsymbol{\rho}[s], t|\tau\}\vec{T}[\boldsymbol{\rho}(s), \tau]\},$$
$$\vec{T} = \mathbf{Nr}\{\Phi'_{\boldsymbol{r}}\{\boldsymbol{\rho}[s(t)], t|\tau\}\vec{T}[\boldsymbol{\rho}(s(t)), \tau]\}.$$

In what follows, $\mathbf{d}$ stands for the differential. Since $\Phi(r, \tau|\tau) \equiv r$ and for infinitesimally small increments,

$$\mathbf{d}\,\mathbf{Nr}[\vec{W}] = \frac{1}{\|\vec{W}\|}\mathbf{Pr}_{\vec{W}^{\perp}}[\mathbf{d}\vec{W}],$$

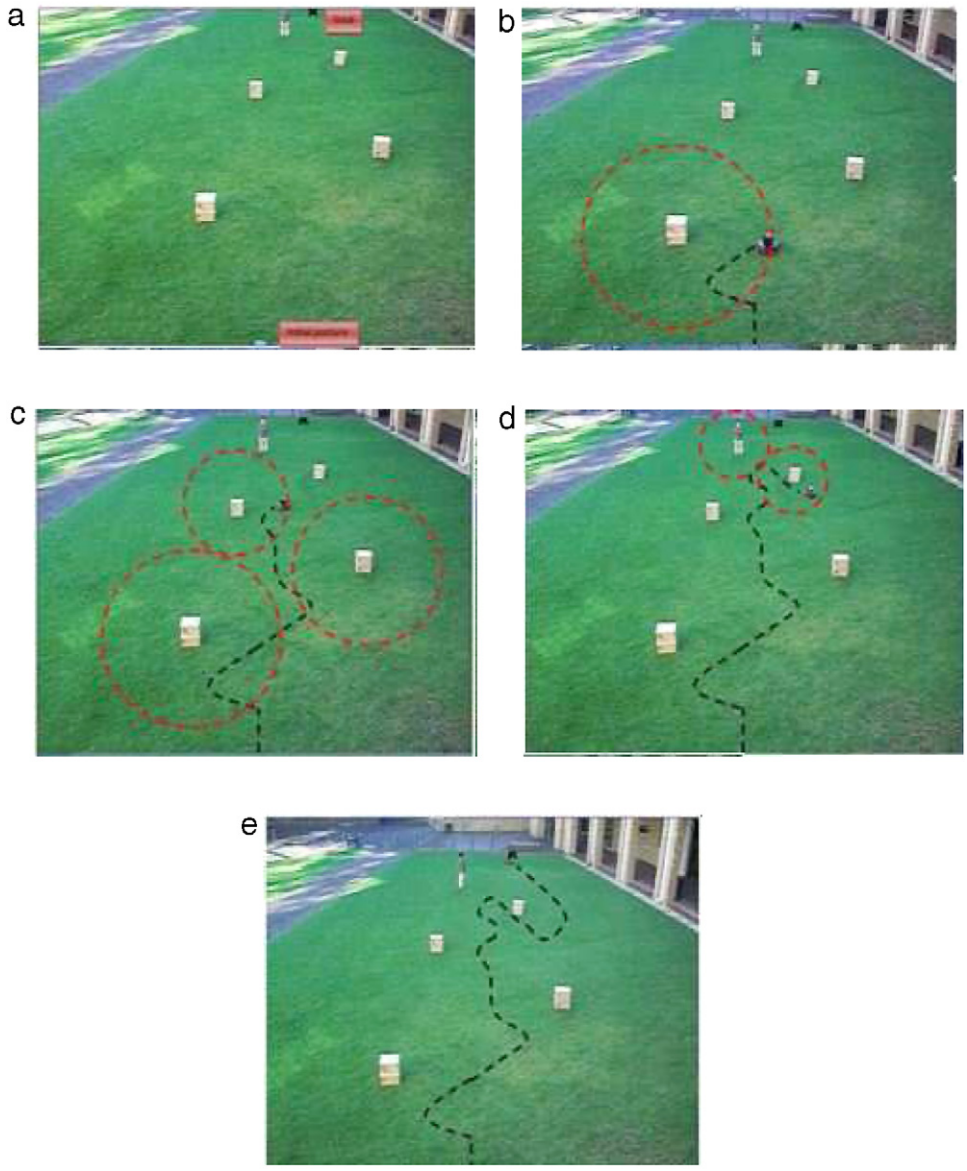


**Fig. 12.** Robot navigation among static obstacles.

we see that for an infinitesimal time increment $t = \tau + \mathbf{d}t$,

$$\begin{aligned}
\mathbf{d}\vec{T} &= \mathbf{Pr}_{\vec{N}(\tau)}[\mathbf{d}\Phi'_{\boldsymbol{r}}\{\boldsymbol{\rho}[s(t)], t|\tau\}\vec{T}\{\boldsymbol{\rho}[s(t)], \tau\}] \\
&= \mathbf{Pr}_{\vec{N}(\tau)}[\Phi'_{\boldsymbol{r}}\{\boldsymbol{\rho}[s(\tau+\mathbf{d}t)], \tau+\mathbf{d}t|\tau\}\vec{T}\{\boldsymbol{\rho}[s(\tau+\mathbf{d}t), \tau]\} \\
&\quad - \Phi'_{\boldsymbol{r}}\{\boldsymbol{\rho}[s(\tau+\mathbf{d}t)], \tau|\tau\}\vec{T}\{\boldsymbol{\rho}[s(\tau+\mathbf{d}t), \tau]\} \\
&\quad + \mathbf{d}\underbrace{\Phi'_{\boldsymbol{r}}\{\boldsymbol{\rho}[s(t)], \tau|\tau\}}_{=I}\vec{T}\{\boldsymbol{\rho}[s(t), \tau]\}] \\
&\overset{(5)}{=} \mathbf{Pr}_{\vec{N}(\tau)}[\Phi''_{\boldsymbol{r}t}\{\boldsymbol{\rho}[s(\tau)], \tau|\tau\}\vec{T}(\tau) + \kappa(\tau)\dot{s}(\tau)\vec{N}[\tau]]\,\mathbf{d}t \\
&\overset{(6)}{=} \mathbf{Pr}_{\vec{N}(\tau)}[\vec{V}'_{\boldsymbol{r}}(\tau)\vec{T}(\tau) + \kappa(\tau)\dot{s}(\tau)\vec{N}(\tau)]\,\mathbf{d}t \\
&= \underbrace{[\langle\vec{V}'_{\boldsymbol{r}}(\tau)\vec{T}(\tau), \vec{N}(\tau)\rangle + \kappa(\tau)\dot{s}(\tau)]}_{\mu}\vec{N}(\tau)\,\mathbf{d}t,
\end{aligned}$$

which implies the first equation from (A.3). The second one is implied by the relations $\vec{N} = \mathscr{R}_{\frac{\pi}{2}}\vec{T}, -\vec{T} = \mathscr{R}_{\frac{\pi}{2}}\vec{N}$. (A.1) is immediate from (A.3) and (A.4). □

By invoking that $\|\vec{v}\| = v$ for the unicycle, we arrive at

$$(\xi + V_T)^2 + (V_N - \dot{d})^2 = v^2. \tag{A.5}$$

**Lemma A.2.** *The following relation holds*

$$\ddot{d} = \xi\mu - u[\xi + V_T] + A_N + \overset{\bullet}{s}\langle\vec{V}'_{\boldsymbol{r}}\vec{T}; \vec{N}\rangle \tag{A.6}$$

$$= -u[\xi + V_T] + A_N + \frac{2\sigma\xi + \kappa\xi^2 - d\sigma^2}{1 + \kappa d}; \tag{A.7}$$

$$\overset{\bullet}{s} = \frac{\xi - d\sigma}{1 + \kappa d}. \tag{A.8}$$

**Proof.** To prove the required relations at a particular time instant $\tau$, we employ the notations introduced in the proof of the previous lemma and consider an infinitesimal time increment $t = \tau + \mathbf{d}t$. Due to (A.1) and (A.3),

$$\begin{aligned}
\mathbf{d}\vec{v} &= (\mathbf{d}\xi)\vec{T} + \xi\mu\vec{N}\mathbf{d}t + \mathbf{d}\vec{V} - \ddot{\eta}\vec{N}\mathbf{d}t + \dot{\eta}\mu\vec{T}\mathbf{d}t \\
&= [(\mathbf{d}\xi) + \dot{\eta}\mu\mathbf{d}t]\vec{T} + [\xi\mu - \ddot{\eta}]\vec{N}\mathbf{d}t + \mathbf{d}\vec{V}.
\end{aligned}$$

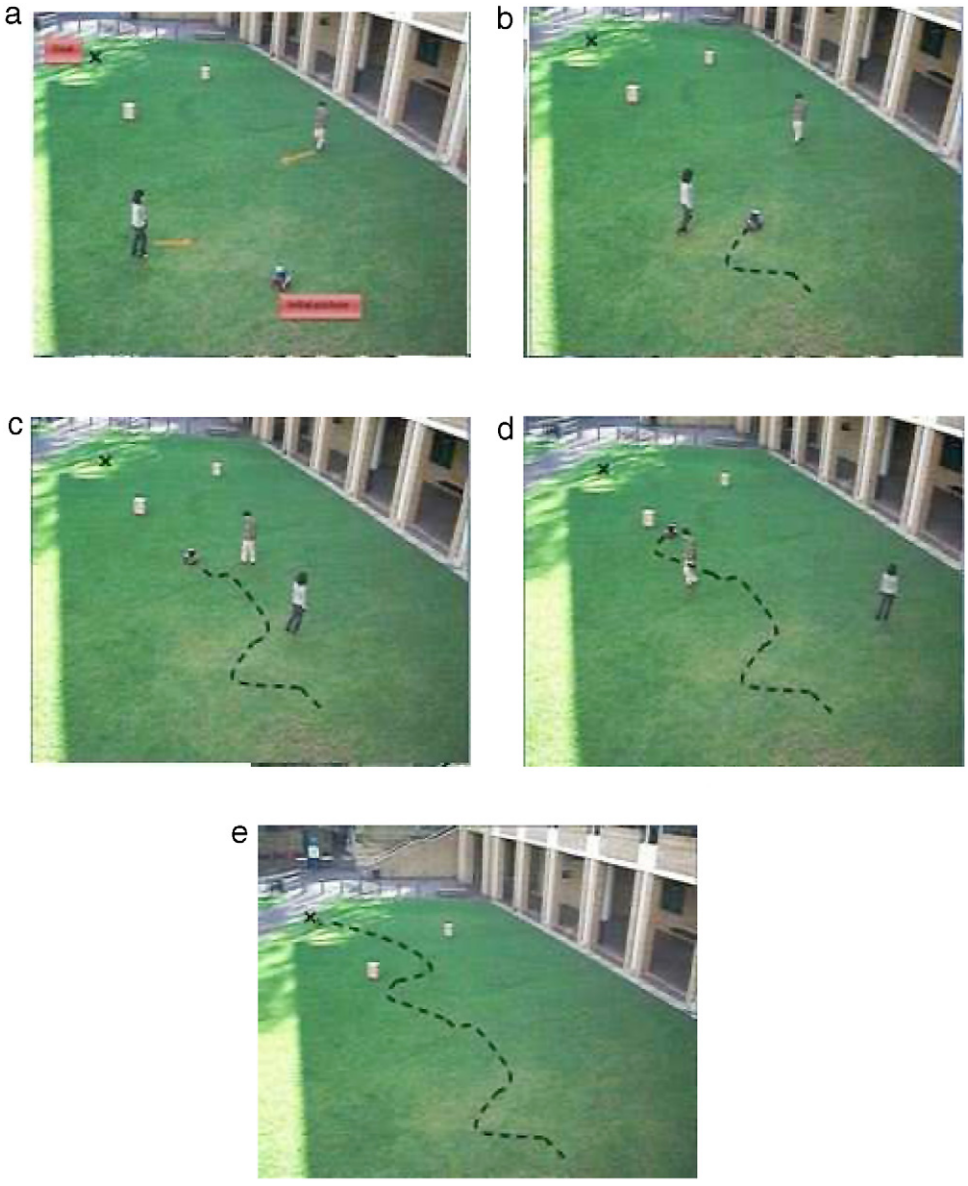


**Fig. 13.** Navigation among static and dynamic obstacles.

Here

$$\begin{aligned}\mathbf{d}\vec{V} &= \vec{V}[\boldsymbol{r}_*(\tau+\mathbf{d}t),\tau+\mathbf{d}t]-\vec{V}[\boldsymbol{r}_*(\tau),\tau]\\ &= \{\vec{V}'_{\boldsymbol{r}}[\boldsymbol{r}_*(\tau),\tau]\dot{\boldsymbol{r}}_*(\tau)+\vec{V}'_t[\boldsymbol{r}_*(\tau),\tau]\}\mathbf{d}t\\ &\overset{(6)}{=} \{\vec{V}'_{\boldsymbol{r}}[\vec{V}+\dot{s}\vec{T}]+\vec{A}-\vec{V}'_{\boldsymbol{r}}\vec{V}\}\mathbf{d}t=\{\vec{A}+\dot{s}\vec{V}'_{\boldsymbol{r}}\vec{T}\}\mathbf{d}t.\end{aligned}$$

Summarizing, we have

$$\mathbf{d}\vec{v}=[(\mathbf{d}\xi)+\dot{\eta}\mu\mathbf{d}t]\vec{T}+[\xi\mu-\ddot{\eta}]\vec{N}\mathbf{d}t+\{\vec{A}+\dot{s}\vec{V}'_{\boldsymbol{r}}\vec{T}\}\mathbf{d}t.$$

On the other hand, (1) implies that

$$\begin{aligned}\mathbf{d}\vec{v} &= u\mathscr{R}_{\frac{\pi}{2}}\vec{v}\mathbf{d}t\overset{(A.1)}{=}u\mathscr{R}_{\frac{\pi}{2}}[\xi\vec{T}+\vec{V}-\dot{\eta}\vec{N}]\mathbf{d}t\\ &= u[\xi\vec{N}+V_T\vec{N}-V_N\vec{T}+\dot{\eta}\vec{T}]\mathbf{d}t.\end{aligned}$$

Equating these two expressions for $d\vec{v}$ yields that

$$u[\dot{\eta}-V_N]=\frac{d\xi}{dt}+\dot{\eta}\mu+A_T+\dot{s}\langle\vec{V}'_{\boldsymbol{r}}\vec{T};\vec{T}\rangle,$$

$$u[\xi+V_T]=\xi\mu-\ddot{\eta}+A_N+\dot{s}\langle\vec{V}'_{\boldsymbol{r}}\vec{T};\vec{N}\rangle\Rightarrow\text{(A.6)}.$$

By (A.1) and (A.2),

$$\xi=\dot{s}+\eta\mu,\quad \mu=\sigma+\kappa\dot{s}\Rightarrow\dot{s}=\frac{\xi-\eta\sigma}{1+\kappa\eta},$$

$$\mu=\frac{\sigma+\kappa\xi}{1+\kappa\eta}.$$

So (A.8) does hold and (A.7) is immediate from (A.6). □

**Corollary A.1.** *Whenever the vehicle travels with $d\equiv d_0$, the parameter $\xi$ is determined by the formula from (8) and*

$$\overline{u}^2v^2\geq V_N^2\overline{u}^2+\left[A_N+\frac{2\sigma\xi+\kappa\xi^2-d_0\sigma^2}{1+\kappa d_0}\right]^2;\tag{A.9}$$

$$\dot{s}=\frac{-V_T\pm\sqrt{v^2-V_N^2}-d_0\sigma}{1+\kappa d_0},\tag{A.10}$$

*where $+$ is taken if the vehicle moves so that the domain is to the left, and $-$ otherwise.*

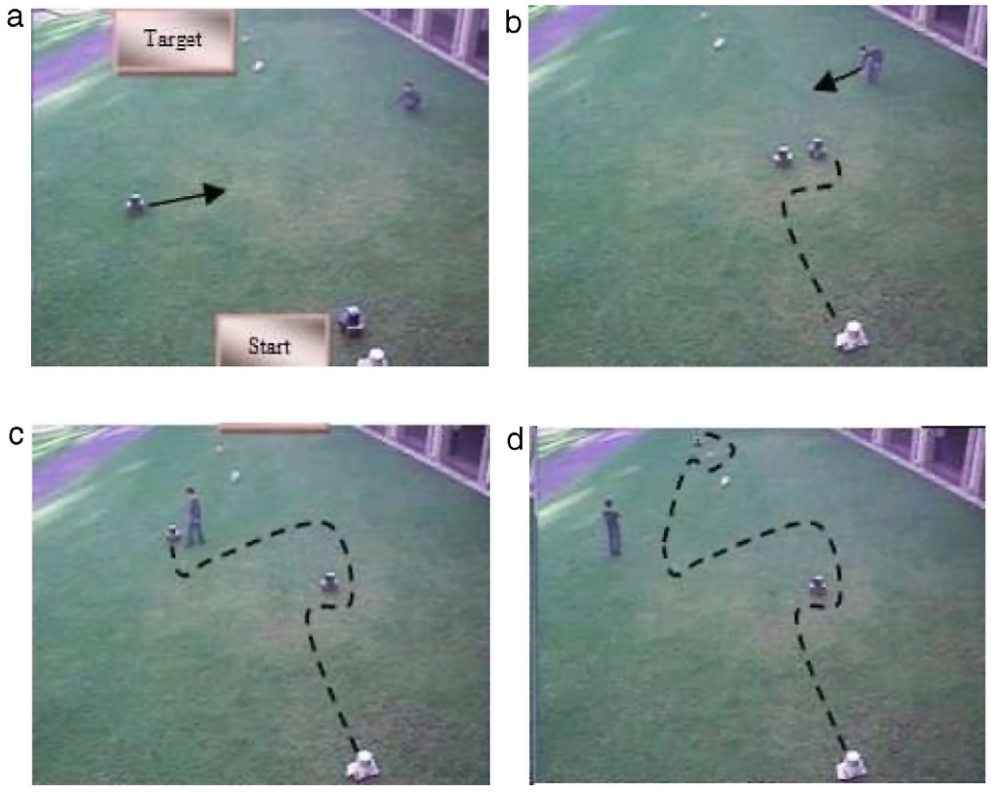


**Fig. 14.** The effect of changing parameters.

**Proof.** By (A.5), $(\xi+V_T)^2+V_N^2=v^2$, which implies the first claim of the lemma. This claim and (A.8) justify (A.10). To prove (A.9), we note that (A.7) shapes into

$$u[\xi+V_T]=A_N+\frac{2\sigma\xi+\kappa\xi^2-d_0\sigma^2}{1+\kappa d_0},$$

and take into account that $|u|\le\overline{u}$. □

**Proof of Lemma 4.1.** The proof is straightforward from Corollary A.1 and (A.8) since $1+d_0\sigma>0$ in (A.8) and overtaking means that $\dot{s}>0$ if the vehicle has the domain to the left, and that $\dot{s}<0$ otherwise. □

The following three lemmas will underlie the proof of Theorem 1. The first of them reveals conditions under which the discontinuous control law (3) exhibits sliding motion.

**Lemma A.3.** *Within the domain $d\in[d_-,d_+]$, the surface $S:=\dot{d}+\chi(d-d_0)=0$ is sliding in the sub-domain*

$$\xi+V_T>0 \tag{A.11}$$

*and two-side repelling in the sub-domain*

$$\xi+V_T<0 \tag{A.12}$$

*if (14) holds. On this surface within the above domain,*

$$|\xi+V_T|\ge v\sqrt{1-(\lambda_v+\eta_v)^2}>0. \tag{A.13}$$

**Proof.** Whenever $S:=\dot{d}-\nu=0$, where $\nu:=-\chi(d-d_0)$, we have by (4),

$$|\dot{d}|=|\nu|\le v_*;\quad |\dot{\nu}|\le\gamma|\dot{d}|=\gamma|\chi(d-d_0)|\le\gamma v_*. \tag{A.14}$$

Due to (A.5)

$$\begin{aligned}|\xi+V_T|&=\sqrt{v^2-(V_N-\dot{d})^2}\ge\sqrt{v^2-(|V_N|+v_*)^2}\\&\overset{(a)}{\ge} v\sqrt{1-(\lambda_v+\eta_v)^2}\Rightarrow\text{(A.13)},\end{aligned} \tag{A.15}$$

where (a) holds due to (10) and (14). Furthermore,

$$\begin{aligned}\dot{S}=&\frac{d}{dt}[\dot{d}+\chi(d-d_0)]=\ddot{d}-\dot{\nu}\\&\overset{(A.7)}{=}-u[\xi+V_T]+A_N+\frac{2\sigma\xi+\kappa\xi^2-d\sigma^2}{1+\kappa d}-\dot{\nu},\end{aligned}$$

where $\xi=-V_T\pm\sqrt{v^2-(V_N-\dot{d})^2}$ by (A.5). So by invoking (12), we see that

$$\dot{S}=[\xi+V_T]\left[-u+\Omega(\boldsymbol{r}_*,t,d,\dot{d})-\frac{\dot{\nu}}{\xi+V_T}\right]. \tag{A.16}$$

Here due to (13),

$$\begin{aligned}\left|\Omega(\boldsymbol{r}_*,t,d,\dot{d})-\frac{\dot{\nu}}{\xi+V_T}\right|\le&\ (\lambda_a+\eta_a)\overline{u}+\frac{\gamma v_*}{|\xi+V_T|}\\&\overset{(A.13)}{\le}(\lambda_a+\eta_a)\overline{u}+\frac{\gamma v_*}{v\sqrt{1-(\lambda_v+\eta_v)^2}}\\&\overset{(14)}{<}\overline{u}.\end{aligned} \tag{A.17}$$

So the signs taken by $\dot{S}$ for $u=\overline{u}$ and $u=-\overline{u}$, respectively, are opposite. In the case (A.11), the sign is opposite to $\mathrm{sgn}u\overset{(3)}{=}\mathrm{sgn}S$; in the case (A.12) the signs are equal. This implies the conclusion of the lemma. □

**Lemma A.4.** *If the equation $\dot{d}+\chi(d-d_0)=0$ becomes true at some time $t_0$ when $d\in[d_-,d_+]$, then monotonically and exponentially fast $d\to d_0,\dot{d}\to 0$ as $t\to\infty$. Furthermore, $d(t)\in[d_-,d_+]$ and (A.11) holds for all $t\ge t_0$.*

**Proof.** Lemma A.3 guarantees that first, $\xi + V_T > 0$ at $t = t_0$ and second, this inequality is still valid and sliding motion occurs while $d \in [d_-, d_+]$. During this motion, $\dot{y} = -\chi(y)$ for $y := d - d_0$, where $\chi(y) \cdot y > 0\ \forall y \neq 0$ and $\chi(0) = 0$. It follows that any solution $d$ of the sliding mode differential equation monotonically converges to $d_0$. At the same time, $d_0 \in [d_-, d_+]$. Hence $d$ will never leave the interval $[d_-, d_+]$, the sliding mode will never be terminated, the inequality $\xi + V_T > 0$ will never be violated, and $d \to d_0, \dot{d} \to 0$ as $t \to \infty$. Application of the Lyapunov's first method to the equation $\dot{y} = -\chi(y)$ at the equilibrium point $y = 0$ shows that the convergence is exponentially fast. □

**Remark A.1.** Lemmas A.3 and A.4 evidently remain true for the control law (15) provided that formulas (A.11) and (A.12) are interchanged in their formulations.

**Lemma A.5.** *Under the assumptions of Theorem 1, both relations $\dot{d} + \chi(d - d_0) = 0, \xi + V_T > 0$ become true at some time $t_0 \in [0, \frac{3\pi}{\bar{u}})$, and for the first such a time, $d \in [d_-, d_+]$.*

**Proof.** If these relations are true initially, the claim is true. Otherwise, $\dot{d} + \chi(d - d_0) \neq 0$ for $t > 0, t \approx 0$, and until the first time $t_0$ when the equation becomes true, the robot moves with the constant control $u \equiv \pm\bar{u}$.

Let $u \equiv \bar{u}$ for the definiteness. Now we analyze the motion of the robot driven by the constant control $u \equiv \bar{u}$ during the time interval $[0, \frac{3\pi}{\bar{u}}]$. This motion is along the +initial circle by Definition 3. By Assumption 7, this circle and the domain $D(t)$ are constantly separated by a steady straight line for $t \in [0, \frac{3\pi}{\bar{u}}]$. So the polar angle of the vector $\vec{h}(t)$ directed from $\boldsymbol{r}_*(t)$ to $\boldsymbol{r}(t)$ continuously evolves over an interval whose length does not exceed $\pi$; see Fig. 7(b). Meanwhile, the polar angle of $\vec{v}(t)$ continuously runs over an interval with the length $3\pi$. Hence there unavoidable exist two time instants $t_i \in [0, \frac{3\pi}{\bar{u}}], i = 1, 2$ such that $\vec{v}(t_i)$ and $(-1)^i\vec{h}(t_i)$ are co-linear and identically directed for $i = 1, 2$. Thanks to (A.1),

$$(-1)^i\dot{d}(t_i) = v + (-1)^i V_N(t_i) \geq v - |V_N| \overset{(10)}{\geq} (1 - \lambda_v)v \overset{(11)}{>} \eta_v v \overset{(14)}{\geq} v_* \overset{\text{Fig. 1(b)}}{\geq} |\chi[d(t_i) - d_0]|.$$

Thus the continuous function of time $S$ assumes values of opposite signs at $t = t_1, t_2$. It follows that $S$ inevitably arrives at zero within $[0, \frac{3\pi}{\bar{u}}]$. Lemma A.3 implies that (A.12) cannot be true at this moment. So (A.11) is true due to (A.13), which and completes the proof. □

**Proof of Theorem 1.** This theorem is immediate from Lemma A.4–Lemma A.5 since (A.11) implies that the angle between $\vec{v}$ and $\vec{T}$ is acute due to (A.1). □

**Proof of Remark 3.** is based on Remark A.1 and consists in merely retracing the above arguments. □

To prove Lemma 5.1, we suppose that only Assumptions 1–5 are true from now on.

**Lemma A.6.** *Let $\mathfrak{D} = [d_-, d_+]$ be a regular interval (not necessarily that from Assumption 6) and let the controller parameters be chosen so that (14) is satisfied with $\lambda_v, \lambda_a$ and $z_*$ taken from (10) and (13), where $d \in \mathfrak{D}$ are considered. Then there exist $\varepsilon > 0, \zeta_v > 0$ and $\zeta > 0$ such that*

$$d \in [d_-, d_+] \wedge |S| < \varepsilon \Rightarrow |\xi + V_T| \geq \zeta_v, \tag{A.18}$$

$$d \in [d_-, d_+] \wedge |S| < \varepsilon \wedge \xi + V_T > 0 \Rightarrow \dot{S}S \leq -\zeta|S|. \tag{A.19}$$

**Proof.** The proof is basically by retracing the arguments from the proof of Lemma A.3. Whenever the premises in (A.18) are true, (A.14) is altered into

$$|\dot{d}| \leq |v| + \varepsilon \leq v_* + \varepsilon; \quad |\dot{v}| \leq \gamma|\dot{d}| \leq \gamma(|v| + \varepsilon) \leq \gamma(v_* + \varepsilon).$$

Hence by taking $\varepsilon > 0$ small enough, we transform (A.15) into

$$|\xi + V_T| \geq v\sqrt{1 - \left(\lambda_v + \eta_v + \frac{\varepsilon}{v}\right)^2} \overset{\varepsilon \approx 0}{\geq} \zeta_v := v\frac{1}{2}\sqrt{1 - (\lambda_v + \eta_v)^2},$$

i.e., (A.18) does hold. Similarly in (A.17), the estimated quantity does not exceed

$$(\lambda_a + \eta_a)\bar{u} + \frac{\gamma(v_* + \varepsilon)}{v\sqrt{1 - (\lambda_v + \eta_v)^2}} \overset{\varepsilon \approx 0}{<} \bar{u}.$$

By bringing the pieces together, we arrive at (A.19). □

Note that (A.18) and (A.19) remains true as $\varepsilon$ decreases. So without any loss of generality, we may assume that $\varepsilon < v_*$.

**Corollary A.2.** *Let $[d_-, d_+] \supset \mathfrak{D}_\varepsilon := \left[d_0 - \frac{\varepsilon}{\gamma}, d_0 + \frac{\varepsilon}{\gamma}\right]$. If $|S| < \varepsilon, d \in \mathfrak{D}_\varepsilon$, and $\xi + V_T > 0$ at some time instant, the system reaches the surface $S = 0$ for no more then $\frac{4S^2(0)}{\gamma}$ time units, not violating the inclusion $d \in \mathfrak{D}_\varepsilon$, and then undergoes sliding motion over this surface.*

**Proof.** Thanks to Lemma A.6, $S^2$ decreases while the system remains in the domain $d \in [d_-, d_+] \wedge |S| < \varepsilon$. Furthermore, in this domain $-\varepsilon - \chi(d - d_0) < \dot{d} < -\chi(d - d_0) + \varepsilon$, where $-\varepsilon - \chi(d - d_0) > 0\ \forall d < d_0 - \frac{\varepsilon}{\gamma}$ and $-\chi(d - d_0) + \varepsilon < 0\ \forall d > d_0 + \frac{\varepsilon}{\gamma}$. Hence $d$ cannot leave the interval $[d_0 - \frac{\varepsilon}{\gamma}, d_0 + \frac{\varepsilon}{\gamma}] \subset [d_-, d_+]$. So the system remains in that domain and $\dot{S}S \leq -\zeta|S|\ \forall t \geq t_0$. It follows that $S^2(t) - S^2(t_0) \leq -4\zeta(t - t_0)$ while the sliding surface $S = 0$ is not reached, which evidently implies the claim. □

**Proof of Lemma 5.1.** By Remark 1, there is a regular interval of the form $[d_-, d_+] = [d_0 - \varepsilon_*, d_0 + \varepsilon_*]$, where $\varepsilon_* > 0$. Lemma A.6 assigns some $\varepsilon > 0$ to this interval. By decreasing $\varepsilon > 0$ if necessary, we can ensure that the assumption of Corollary A.2 holds and $\varepsilon < \varepsilon_0(\gamma + 2)$. The constant $c$ in (16) is picked so that $c < \varepsilon/(\gamma + 1)$. The whenever the premises from (16) hold, $|S| \leq |\dot{d}| + |\chi(d - d_0)| \leq c + \gamma|d - d_0| \leq (1 + \gamma)c < \varepsilon$ and $d \in [d_0 - \frac{\varepsilon}{\gamma}, d_0 + \frac{\varepsilon}{\gamma}]$. Then for $t \geq t_0$, Corollary A.2 guarantees that $|d(t) - d_0| \leq \varepsilon/\gamma < \varepsilon_0$ and $|\dot{d}| = |S - \chi(d - d_0)| \leq |S| + |\chi(d - d_0)| \leq \varepsilon + \gamma|d - d_0| \leq 2\varepsilon < \varepsilon_0$, i.e., the first conclusion from (16) does hold. The second one is immediate from Corollary A.2. □

**Proof of Remark 4.** This remark in straightforward from Theorem 1 and (A.5), (A.8). □

## References


[1] J. Latombe, Robot Motion Planning, Kluwer Academic Publishers, London, 1991.

[2] J. Minguez, L. Montano, Robot navigation in very complex, dense and cluttered indoor/outdoor environments, in: Proc. of the 15th IFAC World Congress, pp. 218–223.

[3] L. Lapierre, R. Zapata, P. Lepinay, Combined path-following and obstacle avoidance control of a wheeled robot, The International Journal of Robotics Research 26 (2007) 361–375.

[4] F. Large, C. Lauger, Z. Shiller, Navigation among moving obstacles using the NLVO: principles and applications to intelligent vehicles, Autonomous Robots 19 (2005) 159–171.

[5] R. Kulić, Z. Vukić, Methodology of concept control synthesis to avoid unmoving and moving obstacles, Journal of Intelligent and Robotic Systems 45 (2006) 267–294.

[6] Z. Qu, J. Wang, C. Plaisted, A new analytical solution to mobile robot trajectory generation in the presence of moving obstacles, IEEE Transactions on Robotics 20 (2004) 978–993.
[7] P. Fiorini, Z. Shiller, Motion planning in dynamic environments using velocity obstacles, International Journal of Robotics Research 17 (1998) 760–772.
[8] T. Fraichard, Trajectory planning in a dynamic workspace: a state-time space approach, Advanced Robotics 13 (1999) 75–94.
[9] J. Reif, M. Sharir, Motion planning in the presence of moving obstacles, Journal of ACM 41 (1994) 764–790.
[10] J. Canny, The Complexity of Robot Motion Planning, MIT Press, Cambridge, MA, 1988.
[11] M. Seder, K. Macek, I. Petrovic, An integrated approach to realtime mobile robot control in partially known indoor environments, in: 31st Annual Conference of the IEEE Industrial Electronics Society, pp. 1785–1790.
[12] D. Fox, W. Burgard, S. Thrun, The dynamic window approach to collision avoidance, IEEE Robotics and Automation Magazine 4 (1997) 23–33.
[13] R. Simmons, The curvature-velocity method for local obstacle avoidance, in: IEEE International Conference on Robotics and Automation, pp. 3375–3382.
[14] Y. Nak, R. Simmons, The lane-curvature method for local obstacle avoidance, in: IEEE International Conference on Robotics and Automation, pp. 1615–1621.
[15] A. Chakravarthy, D. Ghose, Obstacle avoidance in a dynamic environment: a collision cone approach, IEEE Transactions on Systems, Man, and Cybernetics 28 (1998) 562–574.
[16] T. Fraichard, H. Asama, Inevitable collision states. A step towards safer robots? in: IEEE International Conference on Intelligent Robots and Systems, pp. 388–393.
[17] E. Owen, L. Montano, A robocentric motion planner for dynamic environments using the velocity space, in: IEEE International Conference on Intelligent Robots and Systems, pp. 2833–2838.
[18] S. Lindemann, I. Hussein, S.M. LaValle, Real time feedback control for nonholonomic mobile robots with obstacles, in: 45th IEEE Conf. Decision and Control, pp. 2406–2411.
[19] A. Ferrara, M. Rubagotti, Sliding mode control of a mobile robot for dynamic obstacle avoidance based on a time-varying harmonic potential field, in: ICRA 2007 Workshop: Planning, Perception and Navigation for Intelligent Vehicles.
[20] J. Chunyu, Z. Qu, E. Pollak, M. Falash, Reactive target-tracking control with obstacle avoidance of unicycle-type mobile robots in a dynamic environment, in: ACC, pp. 1190–1196.
[21] E. Masehian, Y. Katebi, Robot motion planning in dynamic environments with moving obstacles and target, World Academy of Science, Engineering and Technology 29 (2007) 107–112.
[22] L.E. Dubins, On curves of minimal length with a constraint on average curvature and with prescribed initial and terminal positions and tangents, American Journal of Mathematics 79 (1957) 497–516.
[23] T. Fossen, Guidance and Control of Ocean Vehicles, Wiley, NY, 1994.
[24] E.M.P. Low, I.R. Manchester, A.V. Savkin, A bilogically inspired method for vision-based docking of wheeled mobile robots, Robotics and Autonomous Systems 55 (2007) 769–784.
[25] A. Girard, A.S. Howell, J.K. Hedrick, Border patrol and surveillance missions using multiple unmanned air vehicles, in: Proceedings of the 43th IEEE Conference on Decision and Control, Nassau, Bahamas, pp. 620–625.
[26] K.E. Bekris, A.A. Argyros, L.E. Kavraki, Angle-based methods for mobile robot navigation: reaching the entire plane, in: Proc. IEEE Int. Conf. on Robotics and Automation, ICRA, 2004, pp. 2373–2378.
[27] S.G. Loizou, V. Kumar, Biologically inspired bearing-only navigation and tracking, in: Proceedings of the 46th IEEE Conference on Decision and Control, 2007, pp. 1386–1391.
[28] A. Arora, P. Dutta, S. Bapat, et al., A line in the sand: a wireless sensor network for target detection, classification, and tracking, Computer Networks 45 (2004) 605–634.
[29] A. Gadre, D.J. Stilwell, Toward underwater navigation based on range measurements from a single location, in: Proc. of IEEE Int. Conf. on Robotics and Automation, 2004, pp. 4472–4477.
[30] P.N. Pathirana, N. Bulusu, A.V. Savkin, S. Jha, Node localization using mobile robots in delay-tolerant sensor networks, IEEE Transactions on Mobile Computing 4 (2005) 285–296.
[31] A. Matveev, H. Teimoori, A. Savkin, Range-only measurements based target following for wheeled mobile robots, Automatica 47 (2011) 177–184.
[32] A. Matveev, H. Teimoori, A. Savkin, A method for guidance and control of an autonomous vehicle in problems of border patrolling and obstacle avoidance, Automatica 47 (2011) 515–524.
[33] H. Teimoori, A.V. Savkin, Equiangular navigation and guidance of a wheeled mobile robot based on range-only measurements, Robotics and Autonomous Systems 58 (2010) 203–215.
[34] H. Teimoori, A.V. Savkin, A biologically inspired method for robot navigation in a cluttered environment, Robotica 28 (2010) 637–648.
[35] V.I. Utkin, Sliding Modes in Control Optimization, Springer-Verlag, Berlin, 1992.
[36] J. Ben-Asher, I. Yaesh, Advances in Missile Guidance Theory, AIAA, Inc., Washington, DC, 1998.
[37] E.H. Lockwood, A Book of Curves, Cambridge University Press, 1961.
[38] D.W. Thompson, On Growth and Form, Cambridge University Press, 1966.
[39] V. Tucker, The deep fovea, sideways vision and spiral flight paths in raptors, Journal of Experimental Biology 203 (2001) 3745–3754.
[40] M. Srinivasan, Honeybees as a model for the study of visually guided flight, navigation, and biologically inspired robotics, Physiological Reviews 91 (2011) 413–460.
[41] K. Ahnert, M. Abel, Numerical differentiation of experimental data: local versus global methods, Computer Physics Communications 177 (2007) 764–774.
[42] L.K. Vasiljevic, H.K. Khalil, Error bounds in differentiation of noisy signals by high-gain observers, Systems & Control Letters 57 (2008) 856–862.
[43] V. Arnold, The Theory of Singularities and its Applications, second ed., The Press Syndicate of the University of Cambridge, Cambridge, 1993.
[44] J. Spencer, Continuum Mechanics, Dover Publications, NY, 2004.
[45] J. Thorpe, Elementary Topics in Differential Geometry, Springer, NY, 1979.

**Alexey S. Matveev** was born in Leningrad, USSR, in 1954. He received the M.S. and Ph.D. degrees in 1976 and 1980, respectively, both from the Leningrad University. Currently, he is a professor of the Department of Mathematics and Mechanics, Saint Petersburg University. His research interests include estimation and control over communication networks, hybrid dynamical systems, and navigation and control of mobile robots.

**Chao Wang** was born in 1987 in China. He received his B.E. Degree (Hons Class 1) in 2009 from University of New South Wales (UNSW). He is currently following his research as a Ph.D. student in UNSW. His research interests include control system analysis, nonholonomic system, and navigation of wheeled mobile robot in cluttered dynamic environment.

**Andrey V. Savkin** was born in 1965 in Norilsk, USSR. He received the M.S. and Ph.D. degrees from the Leningrad State University, USSR in 1987 and 1991, respectively. From 1987 to 1992, he was with the Television Research Institute, Leningrad, USSR. From 1992 to 1994, he held a postdoctoral position in the Department of Electrical Engineering, Australian Defence Force Academy, Canberra. From 1994 to 1996, he was a Research Fellow with the Department of Electrical and Electronic Engineering and the Cooperative Research Center for Sensor Signal and Information Processing at the University of Melbourne, Australia. In 1996–2000, he was a Senior Lecturer, and then an Associate Professor with the Department of Electrical and Electronic Engineering at the University of Western Australia, Perth. Since 2000, he has been a Professor with the School of Electrical Engineering and Telecommunications at the University of New South Wales, Sydney, Australia. His current research interests include robust control and state estimation, hybrid dynamical systems, guidance, navigation and control of mobile robots, applications of control and signal processing in biomedical engineering and medicine. He has authored/co-authored five research monographs and numerous journal and conference papers on these topics. He has served as an associate editor for several international journals.